UNIVERSIDADE DE SÃO PAULO
Instituto de Física de São Carlos

Proceedings of the seminar to the course

Fundamentos da Interação da Radiação com a Matéria

SFI5905 / 2023-1

Ph.W. Courteille (editor)
Universidade de São Paulo
Instituto de Física de São Carlos
27/06/2023

.

Contents

Preface

Estes anais (ou proceedings) reúnem as monografias elaboradas pelos alunos do curso de Fundamentos da Interação da Radiação com a Matéria (SFI5905), realizado no Instituto de Física de São Carlos da Universidade de São Paulo durante o primeiro semestre de 2023 sob supervisão do Prof. Ph. W. Courteille.

1

Quantum gates

Anna Cristina Cavallari Inacio

Instituto de Física de São Carlos, Universidade de São Paulo, 13560-970 São Carlos, SP, Brazil

Abstract: Quantum computing is an area that awakens the interest of a lot of people either they work with science and technology or not. This paper aim is to brief discuss quantum gates, a really important concept for quantum computing. In this we describe the concept of qubits, how quantum gates transform them, by studying the most common and useful gates, and introduce quantum circuits and their importance to the development of quantum computers.

1.1 Introduction

With the advance of quantum mechanics, surfaced an interest in understand and manipulate quantum systems and one of the proposed ways resulted in what we know today about quantum computing and quantum information. In the beginning of the 80's the physicist Paul Benioff suggests that quantum mechanics can be used in computing by proposing a quantum mechanical model of the Turing Machine, the base for classic computing now days. Later, Richard Feynman pointed out that simulating quantum mechanics systems on classical computers is a extremely difficult task, mostly in terms of time, and suggested that computers based on quantum mechanics would allow us to avoid the difficulties since it would have greater power than the classic one [1]. Based on this, in the next decades, several teams of researchers began to study the use of quantum systems in computing. Currently, in 2019, Google AI claimed to have achieved quantum supremacy, solving in 200 seconds an operation that would be infeasible on any classical machine, even supercomputers[2]. The first challenge for quantum computing is to understand what is the quantum bit (qubit), analogous to the bit of classical computing, and the quantum logic gates that make up the quantum circuits responsible for the operation of quantum computers. This work aim to study a description of qubits and some of the most important quantum gates and explore a little how basic quantum circuits function

1.2 Quantum Bits

In classical computation, the bit is a binary digit that is the fundamental state for storing information, assuming the value 0 or 1. Analogously, in the area of quantum computing or quantum information, this role is fulfilled by a unit named quantum bit or qubit. The qubit has two possible states $|0\rangle$ and $|1\rangle$, that correspond to the classical ones, however, it also can be linear combinations of these states, which we call in quantum mechanics a superposition, given by [3]:

$$|\psi\rangle = \alpha\,|0\rangle + \beta\,|1\rangle \tag{1.1}$$

where α and β are complex numbers. The state of a qubit is a vector in a two-dimensional complex vector space and the states $|0\rangle$ and $|1\rangle$ are computational basis states that form an orthonormal basis for this vector space. A useful way to visualize the state of a qubit is geometric representation through the Bloch sphere how it is showed in Fig. 2.1.

Because $|\alpha|^2 + |\beta|^2 = 1$, we can rewrite Eq. 2.1 as

$$|\psi\rangle = \cos\frac{\theta}{2}\,|0\rangle + \exp\{i\varphi\}\sin\frac{\theta}{2}\,|1\rangle \tag{1.2}$$

where θ and φ define a point on the unite sphere. The computational basis states lie on the z-axis.

For measuring the bit value in the computational basis, we must determine the alignment of its spin with respect to the z-axis. If the qubit is aligned

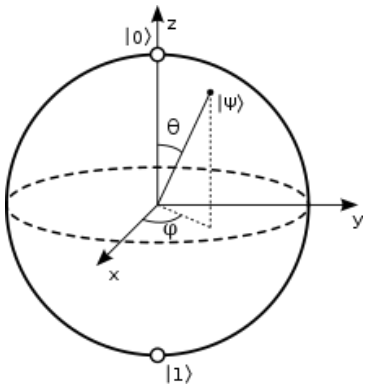

Figure 1.1: Qubit state $|\psi\rangle$ represented by a point on Bloch sphere. Its parameters are θ and φ

"spin-up" it s in the state $|0\rangle$, and if it is aligned "spin-down" it is in the state $|1\rangle$. In a more general way, the result of a measuring is a probability that depends on the values of α and β, so we get either the result 0, with a probability $|\alpha|^2$, or the result 1, with a probability $|\beta|^2$, where, as said before, $|\alpha|^2 + |\beta|^2 = 1$.

1.3 Quantum Gates

The classic logic gates are a way the bits can be stored or transformed creating new information. There are three basic logic gates, each of them has two entry bits and produces one exit: the gate NOT, that flips the state of the bit, changing 0 to 1 and 1 to 0; the gate OR, that returns 1 if one of the entries is equal to 1; and the gate AND, that returns 1 only if both entries are equal to the value 1 and returns 0 any other case. Quantum gates follow the same principle, operating on n qubits. Quantum gates are unitary operators described as unitary matrices relative to some basis. Lets consider a logic gate represented by the U operator, if we apply $U^\dagger$ in the final state we obtain the initial one: $U^\dagger |\psi_f\rangle = U^\dagger U = |\psi_i\rangle$, i.e. $U^\dagger U = \mathbb{I}$ and U is a unitary operator. This means that unitary operators are reversible. How discussed previously, quantum gates are unitary operators, therefore they are reversible, we can undo a gate using the output qubit to obtain the initial one. This is a very important propriety. Exists an uncountable number of gates, some of them more important and known than others and below we will see a brief discussion of some of them.

1.3.1 Single qubit logic gate

Pauli Gates

The first Pauli Gate comes from the Pauli X matrix and is equal with the classical NOT gate. We can represent the NOT gate in matrix form as

$$X = \begin{bmatrix} 0 & 1 \\ 1 & 0 \end{bmatrix} \tag{1.3}$$

It "negates" the computational basis states $|0\rangle$ and $|1\rangle$ when applied, so the corresponding output from NOT gate acting on a superposition state is given by

$$X \begin{bmatrix} \alpha \\ \beta \end{bmatrix} = \begin{bmatrix} \beta \\ \alpha \end{bmatrix} \tag{1.4}$$

If we apply this gate one more time, we return to the initial state, thus $XX = \mathbb{I}$. The next one, naturally, comes from the Pauli Y gate

$$Y = \begin{bmatrix} 0 & -i \\ i & 0 \end{bmatrix} \tag{1.5}$$

And the corresponding output is

$$Y \begin{bmatrix} \alpha \\ \beta \end{bmatrix} = i \begin{bmatrix} \beta \\ -\alpha \end{bmatrix} \tag{1.6}$$

We also have the gate from Pauli Z matrix, that acts inverting the signal of the computational basis state $|1\rangle$ and maintaining the $|0\rangle$ the same

$$Z = \begin{bmatrix} 1 & 0 \\ 0 & -1 \end{bmatrix} \tag{1.7}$$

$$Z \begin{bmatrix} \alpha \\ \beta \end{bmatrix} = \begin{bmatrix} \alpha \\ -\beta \end{bmatrix} \tag{1.8}$$

Both previous gates, return to initial state if applied two times, thus, $YY = \mathbb{I}$ anf $ZZ = \mathbb{I}$ We can represent quantum gates graphically, as shown in Fig 2.2. The qubit entry is represented by a horizontal line in the left side of the box (gate) and the output is the horizontal line on the other side. This assembly is what we know as a very simple quantum circuit. We will study quantum circuits with more depth latter on this work.

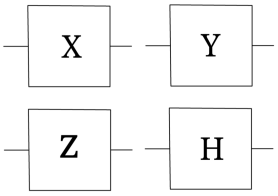

Figure 1.2: Graphically representation of the most used single qubit gates. From left to right and top to bottom, Pauli gates X, Y, Z and Hadarmad gate H. Qubits are represented by the horizontal lines and the gates by the box.

Hadarmad Gate

One of the most useful single qubit gates is the Hadamard gate, H, defined by the matrix

$$H = \frac{1}{\sqrt{2}} \begin{bmatrix} 1 & 1 \\ 1 & -1 \end{bmatrix} \tag{1.9}$$

When the H gate acts on the computational basis states it transforms them into a superposition state, which is a very powerful operation in quantum computing. By applying in parallel, a separate Hadamard gate to each of n qubits, each in the state $|0\rangle$, we can create an n-qubit superposition containing 2^n component eigenstates, giving the quantum computer its ability to load exponentially many indices only using polynomially many operations, increasing the computing velocity compered to the best classical algorithms [4].

$$H|0\rangle = \frac{1}{\sqrt{2}}(|0\rangle + |1\rangle) \tag{1.10}$$

$$H|1\rangle = \frac{1}{\sqrt{2}}(|0\rangle - |1\rangle) \tag{1.11}$$

Just like the other single bit gates, if a qubit passes through the Hadamard gate twice consecutively it returns to the original state, $HH = \mathbb{I}$

1.3.2 Two qubit logic gate

Let $|00\rangle, |01\rangle, |10\rangle, |11\rangle$ be a basis for two-qubit systems.

controlled-NOT gate

The controlled-NOT gate, or CNOT gate, is a very important gate for quantum computation. The gate flips the second qubit, called target qubit, when the first qubit, called control qubit, is $|1\rangle$. It can be represented in the following matrix form

$$U_{CNOT} = \begin{bmatrix} 1 & 0 & 0 & 0 \\ 0 & 1 & 0 & 0 \\ 0 & 0 & 0 & 1 \\ 0 & 0 & 1 & 0 \end{bmatrix} \tag{1.12}$$

The action of the controlled-NOT gate is given by

$$U_{CNOT} : |00\rangle \mapsto |00\rangle, |01\rangle \mapsto |01\rangle, \tag{1.13}$$

$$|10\rangle \mapsto |11\rangle, |11\rangle \mapsto |10\rangle \tag{1.14}$$

Graphically, a CNOT gate is expressed as shown in Fig y, being $\bullet$ the control bit, while $\oplus$ is the conditional negation.

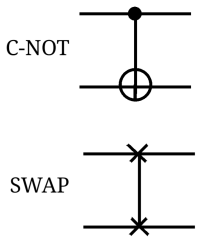

Figure 1.3: Graphically representation of two-qubit gates CNOT gate, in the top, and SWAP gate, in the bottom.

SWAP gate

The SWAP gate, as the name indicates, swaps the states. The matrix is given by

$$U_{SWAP} = \begin{bmatrix} 1 & 0 & 0 & 0 \\ 0 & 0 & 1 & 0 \\ 0 & 1 & 0 & 0 \\ 0 & 0 & 0 & 1 \end{bmatrix} \tag{1.15}$$

It acts as a linear operator on a superposition of states as

$$U_{SWAP}|\psi_1, \psi_2\rangle = |\psi_2, \psi_1\rangle \tag{1.16}$$

1.3.3 Three-qubit logic gate

Let $|000\rangle, |001\rangle, |010\rangle, |011\rangle, |100\rangle, |101\rangle, |110\rangle, |111\rangle$ be a basis for three-qubit systems.

Toffoli gate

The Toffoli gate has three inputs, and the third qubit flips if only the first two qubits are both in the state $|1\rangle$. Because of this behaviour, it is also called the controlled-controlled-NOT gate (CCNOT). The matrix representation is given by

$$U_{CCNOT} = \begin{bmatrix} 1 & 0 & 0 & 0 & 0 & 0 & 0 & 0 \\ 0 & 1 & 0 & 0 & 0 & 0 & 0 & 0 \\ 0 & 0 & 1 & 0 & 0 & 0 & 0 & 0 \\ 0 & 0 & 0 & 1 & 0 & 0 & 0 & 0 \\ 0 & 0 & 0 & 0 & 1 & 0 & 0 & 0 \\ 0 & 0 & 0 & 0 & 0 & 1 & 0 & 0 \\ 0 & 0 & 0 & 0 & 0 & 0 & 0 & 1 \\ 0 & 0 & 0 & 0 & 0 & 0 & 1 & 0 \end{bmatrix} \quad (1.17)$$

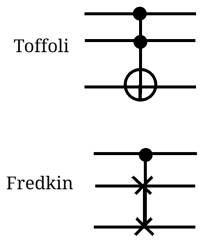

Figure 1.4: Graphically representation of three-qubit gates Toffoli gate, in the top, and Fredkin gate, in the bottom.

Fredkin gate

Under the action of the Fredkin gate the second and third qubits are swapped if and only if the first qubit is in the $|1\rangle$ state. In another words, the Fredkin gate is the controlled-SWAP gate (CSWAP) and is given by the matrix

$$U_{CSWAP} = \begin{bmatrix} 1 & 0 & 0 & 0 & 0 & 0 & 0 & 0 \\ 0 & 1 & 0 & 0 & 0 & 0 & 0 & 0 \\ 0 & 0 & 1 & 0 & 0 & 0 & 0 & 0 \\ 0 & 0 & 0 & 1 & 0 & 0 & 0 & 0 \\ 0 & 0 & 0 & 0 & 1 & 0 & 0 & 0 \\ 0 & 0 & 0 & 0 & 0 & 0 & 1 & 0 \\ 0 & 0 & 0 & 0 & 0 & 1 & 0 & 0 \\ 0 & 0 & 0 & 0 & 0 & 0 & 0 & 1 \end{bmatrix} \quad (1.18)$$

1.4 Quantum circuits

A quantum computation on n qubits requires several quantum gates. We call the organization of these gates a quantum circuit. A quantum circuit is represented by a diagram in which the qubits are the horizontal rails and, by convention, are organized in a way the most significant qubit is on the top rail and the least significant qubit is on the bottom rail. Times flows from left to right in the quantum circuit, so the gates, following the graphic representation already discussed in this work, applied first are shown more to the left than the applied later [4].

Quantum gates can be applied sequentially, in parallel or conditionally. If several gates act upon the same subset of qubits, then those gates must be applied sequentially, i.e. in series, and their final product is computed using the dot product. Suppose we have three quantum gates A, B, C, if A acts before B and B acts before C, their overall effect is computed by their reverse order, $C \bullet B \bullet A$.

When adjacent gates act on independent subsets of the qubits, those gates are applied simultaneously in parallel. The net effect of parallel gates is given by the direct product of matrices, e.g. $A \otimes B$. An important observation is that when a j-qubit quantum gate U acts on a subset of the qubits and there is no explicit operation on the other quibits, mathematically, this can be considered as parallel gate operation in which an i-qubit identity gate ("no-op") is applied to qubits 1 through i, the U gate is applied to qubits $i+1$ through $i+1+j$, and a k-qubit identity gate ("no-op") is applied to qubits $i+1+j$ through $i+j+k$. The final effect of them is $\mathbb{I}_{2^i} \otimes U \otimes \mathbb{I}_{2^k}$, where $\mathbb{I}_{2^l}$ is a $2^l \times 2^l$ dimensional identity matrix [4].

For cases where one subset of qubits (controls) dictate what gate is to be applied to some other subset of qubits (targets) is said the gates are applied conditionally. Mathematically, the operation for composing gates is the direct sum of matrices.

The last thing to discuss in this work is that we can measure the complexity of quantum circuit. It can be characterize in: width, the total number of qubits on which the circuit acts; size, the total number of gates the circuit uses; and length, the number of serial gate operations after having making the circuit the most parallel possible. For a quantum circuit to be considered efficient in performing a computation, any of the complexity parameters has to only grow as a polynomial function. For quantum computing advance, the complexity needed to achieve some computation must be significantly less than the need to achieve the same computation

classically. Ideally the quantum circuit complexity would grow as polynomial function in size and the complexity of the corresponding classical circuit would grow exponentially in size. Although this is not yet possible, there are several research teams striving to improve quantum computing and, hopefully, in the coming decades we will be able to see a significant breakthrough in the area.

1.5 Conclusion

This work discusses what is a qubit and provides a brief description of them, discusses quantum gates, exploring the most important single quibit, two-qubit and three-qubit gates and their mechanism, and introduce the concept of quantum circuits and what is their importance in the advance of quantum computing . All concepts explored here are introductory to better understand quantum computing and other subjects that are developing from it, and, possibly are going to be hot topics of discussion in the scientific and global community in the coming decades.

Bibliografia

[1] Richard P Feynman. Simulating physics with computers. *Feynman and computation.*Pages 133-153. CRC Press, 2018.

[2] Frank Arute, Kunal Arya, Ryan Babbush, Dave Bacon, et al. Quantum supremacy using a programmable superconducting processor. *Nature.*574(7779):505-510, 2019.

[3] Michel A Nielsen and Isaac Chuang. Quantum computing and quantum information. 2002.

[4] Colin P Williams. Explorations in Quantum Computing. *Springer London.* 2010.

[5] Philippe W Courteille. Quantum Mechanics applied to Atomic and Light. *Universidade de São Paulo.* 2023.

2

Schrödinger's cat

Clara Andrade Sapio

Instituto de Física de São Carlos, Universidade de São Paulo, 13560-970 São Carlos, SP, Brazil

Abstract: "Schrödinger's cat" it's an expression known by many since the first contact with Quantum Mechanics. Because of the fact that this subject it's familiar even for lay people, many aspects of our comprehension about this theme are superficial, even for those who had a basic Quantum Mechanics course in the University: the majority does not even know what is the history behind this paradox and the infinity number of questions that resulted from this experimental thought. In this work, will be discussed the historical aspect behind this "problem" and the main hypothesis that has emerged to explain what is the flaw in this experiment. Questions about the "Collapse Theory", "Hidden Variables" and the "Many Words Interpretation" will be discussed in the light of Quantum Mechanics, clarifying the historical, philosophical and mathematical aspects behind the initial "cat" until the "modern cats" that we heard about even nowadays.

2.1 Introduction

The Schrödinger's cat is a paradox that can arises from basically any quantum measurement. If we take a Stern-Gerlach apparatus and perform a measure of the deflection of a spin indicator pointer, we will see that depending on the initial state, the time evolution operator results in a final state $|\psi(T)\rangle$ that represents the superposition of two orthogonal states [2]. Although superpositions are common in Quantum Mechanics, it is weird to have a superposition of opposite directions to identify the position of a pointer, so there it must be some theory to explain what is the logical behind this result.

To resolve this question, Von Neumann postulated that when a measurement is complete, the superposition of positions collapses to a definite position and in this case of the pointer, each one of the orthogonal states have equal probability to appear as the final complete measurement.

At first, this hypothesis seems to resolve the problems through the introduction of this interpretation of Quantum Mechanics collapse. But many questions arise from this postulate: What is a "complete" measure? What is a measuring device? There is a factor of human consciousness interfering in the collapse of a state vector to a definite position?

To complete this set of questions and propose another perspective of the problem, Schrödinger summarize it with a thought experiment, enunciated as it follows: "A cat is placed in a steel chamber, together with the following hellish contraption (which must be protected against direct interference by the cat): In a Geiger counter there is a tiny amount of radioactive substance, so tiny that maybe within an hour one of the atoms decays, but equally probably none of them decays. If one decays then the counter triggers and via a relay activates a little hammer which breaks a container of cyanide" [2]. So after an hour there is an equal chance of finding the cat alive or dead. Mathematically, we have a initial state $|\psi(0)\rangle$:

$$|\psi(0)\rangle = |undecayed\rangle \otimes |untriggered\rangle \otimes |unactivated\rangle \otimes |unbroken\rangle \otimes |alive\rangle \tag{2.1}$$

After a time T equal to an hour, unitary evolution transforms $|\psi(0)\rangle|$ into:

$$\begin{aligned}|\psi(T)\rangle = \tfrac{1}{\sqrt{2}}\,|undecayed\rangle \otimes |untriggered\rangle \\ \otimes |unactivated\rangle \otimes |unbroken\rangle \otimes |alive\rangle \\ + \tfrac{1}{\sqrt{2}}\,|decayed\rangle \otimes |triggered\rangle \otimes \\ |activated\rangle \otimes |broken\rangle \otimes |dead\rangle\end{aligned} \tag{2.2}$$

Figure 2.1: Schematic view of orthogonal alive and dead states of the cat. Reference: [7]

In this case, the collapse postulate applies and the cat has equal probabilities of being alive or being dead or the cat is in a alive-dead state that does not collapse?

In the orthodox Copenhagen interpretation of Quantum Mechanics, we can quote Jordan when he said [1] "observations not only disturb what has to be measured, they *produce* it. In a measurement of a position, the electron is forced to a decision. We compel it to assume a definite position; previously it was neither here nor there, it had not yet made its decision for a definite position...". In the cat paradox, does it mean that the act of the observation (or measure) forces the cat to assume a position, so in this case we can be murdering the cat just by looking at the steel chamber? If it does, how can we define the consciousness of the measure and the exact moment that it has some effect on the state of the cat?

In an attempt to resolve all of the questions that emerged from the Schrödinger's cat paradox, will be highlighted three possibilities of arguments, divided and explained in the sections 3.2, 3.3 and 3.4.

2.2 Quantum Mechanics is incomplete and there is collapse

In this perspective, we will consider two main proposals and give a short explanation with the main ideas about each one.

2.2.1 Von Neumann's Infinite Regress/Chain

In contrast with Bohr's approach, Von Neumann considers the measuring apparatus as a quantum system [1]. If a system S is initially in an eigenstate of the measured observable A with eigenvalue a, some pointer P of the measurement apparatus M gives the position that obtains a as the result after the interaction. But if the system S is initially in a superposition of states, the linear Schrödinger equation predicts that the whole system $S + M$ reaches a linear superposition after the interaction and this situation is described as *quantum entanglement*.

To solve this problem, one can use another measurement apparatus M' to determine the position of the pointer of M, but the process repeats itself and the linearity of Schrödinger equation leads to another superposition. If we use a infinite number of measurement apparatuses $M', M'', ...$, we create a infinite chain of superpositions created by Schrödinger's equation.

In practice, we know that we always observe only one single result in a single experiment, i.e, linear superpositions resolve themselves before they reach the macroscopic world involving the measurement apparatus, so it has to be a theory that break this infinite Von Neumann's chain (collapse). From his observations, he concludes that is not possible to formulate the laws of Quantum Mechanics in a complete and consistent way without reference to human consciousness, because this human factor could be entering the superposition and somehow forcing the system to collapse and give a single result.

Wigner also noticed that we never find ourselves in a superposition state, even though Quantum Mechanics sometimes predicts this fact. In this perspective and agreeing with Von Neumman's observations, Wigner suggested that collapse occurs whenever a conscious human being observes a measuring device in a superposed state. A paradoxical situation expressed by Wigner is the classical "Wigner's friend", when we see this notions of collapse of the state with the interference of the "human consciousness" [1].

The problem about this suggestion resides on the fact that we don't have a well defined concept of what is this "collapse" and specially we don't have the a definition to the concept of "consciousness", but, despite this open problems, we can say that the theories that were explained in this subsection agree with the fact that Quantum Mechanics is incomplete and there has to be collapse of the states, this being one of the forms to interpret Quantum Mechanics in order to "resolve" the cat paradox.

2.2.2 Spontaneous Localization and Continuous Spontaneous Localization

Spontaneous Localization (SL) and Continuous Spontaneous Localization (CSL) are theories that also agree with the fact that Quantum Mechanics

is incomplete and there is collapse. In both models, extended states of matter spontaneously collapse to localized states of size $a \approx 10^{-5} cm$ [2].

In the SL model, an extended state $\psi(x)$ can spontaneously localize to $\psi(x)g(x-\overline{x})$, where $g(x-\overline{x})$ is a gaussian of width a centered at $x = \overline{x}$. The probability of such a localization is consistent with Born's statistical interpretation of the wavefunction, given by the integral:

$$\int d^3x |\psi(x)g(x-\overline{x})|^2 \tag{2.3}$$

The answer of the SL model is that $\psi(x)$ spontaneously collapses at a rate of once in about 300 million years on average ($\lambda = 10^{-16}$). So, in practice, the wavefunction for a single given particle never collapses [2].

However, if we are working with a macroscopic object such as a pointer of a measurement apparatus, the device contains many particles ($\approx 10^{22}$). If we take one particle of a pointer in a superposition of two positions separated by a distance $L \gg a$, we can express the initial state as:

$$|\psi(0)\rangle = \frac{1}{\sqrt{2}}[|0\rangle + |L\rangle] \tag{2.4}$$

To encompass all particles, we can index each one by i and let $|\psi_0^{(i)}\rangle$ and $|\psi_L^{(i)}\rangle$ represent the complete wave function of the i-th particle in the pointer when the pointer position is 0 and L. Let us take the terms $|0\rangle$ and $|L\rangle$ to be tensor products of these one-particle wave functions. Then, we get:

$$|\psi(0)\rangle = \frac{1}{\sqrt{2}}[\bigotimes_i |\psi_0^{(i)}\rangle + \bigotimes_i |\psi_L^{(i)}\rangle] \tag{2.5}$$

If one of this i-particles spontaneously localizes, its wavefunction collapses to a region of size $a \ll L$ and the new wavefunction could overlap with $|\psi_0^{(i)}\rangle$ or $|\psi_L^{(i)}\rangle$, but not both, so the other one would vanish. Considering 10^{22} particles, the rate of this process would be $10^{22} \times 10^{-16} s^{-1} = 10^6 s^{-1} \rightarrow 10^{-6} s$ and this means that the collapse of any macroscopic object would be very quick.

In the CSL model, the time evolution is continuous rather than sudden. An operator $\rho(x,t)$ represents the number of particles in a sphere of radius $a \approx 10^{-5} cm$, centered at x at time t. The evolution of a state vector depends on $\rho(x,t)$ and also on a classical field $w(x,t)$ with a probability density for each spacetime configuration of $w(x,t)$. The evolution equation for $|\psi_w(t)\rangle$, a multi-particle wavefunction could be expressed as:

$$\frac{\partial}{\partial t}|\psi_w(t)\rangle = -\frac{i}{\hbar}H|\psi_w(t)\rangle$$
$$-\frac{1}{4a^3\lambda}\int dx[w(x,t) - 2\lambda\rho(x,t)]^2 |\psi_w(t)\rangle \tag{2.6}$$

This equation represents a nonunitary evolution of the wavefunction to each configuration of $w(x,t)$. In this way, the probability density that the initial state vector actually evolves according to $\psi_w(t)$ is $\langle\psi_w(t)|\psi_w(t)\rangle$ times the probability density for the configuration of $w(x,t)$.

To exemplify the CSL model, we can take $H = 0$ and consider a measuring device with a pointer consisting of a steel needle, $1cm$ long, with cross section $2 \times 10^{-3} cm^2$. The operator $\rho(x,t)$ acts in a way that for a specific point of the pointer it yields the total number of the particles (N) in the sphere of radius a and zero elsewhere.

This way, to cancel the integral on equation 2.6, we must have $w(x,t) = 2\lambda N$ at the position of the undisplaced pointer, and zero elsewhere or at the position of the pointer displaced by L, and zero elsewhere. In the first case, $|\psi(0)\rangle$ evolves to the state $|0\rangle = \bigotimes_i |\psi_0^{(i)}\rangle$ and in the second case $|\psi(0)\rangle$ evolves to the state $|L\rangle = \bigotimes_i |\psi_L^{(i)}\rangle$ and the collapse takes a time $t \approx 10^{-18} s$ to occur [2].

The CSL model is, so far, consistent with experiment. In both models, there is a prediction that the collapse of macroscopic or multi-particle system will occur extremely rapid.

2.3 Quantum Mechanics is incomplete and there is no collapse

An attempt to solve the paradoxes that where haunting classical interpretations of Quantum Mechanics is the theory that became known as "Hidden Variables". This name refers to the parameters that do not appear directly in the wavefunction, but are the ones that complete the quantum description of a system. Therefore, this theory also predicts that the wave function is not a complete description of a system and the "collapse" of a state is reinterpreted.

The greater rupture with the orthodox interpretation of Quantum Mechanics is the fact that the Hidden Variables Theory assumes that there are some pre existing states and the measure does not

"force" the system to make a decision, being just a way to reveal this pre existing properties of the system. With this interpretation, we do not need to worry about the definition of the human consciousness because it is not something that affects directly the measure of the observable.

The meaning of the wavefunction in this theory is to determine the statistical distribution of the variables. In this statistical interpretation, the collapse of the wavefunction is just a readjustment of the probabilities and it goes like this: in the superposed "dead-alive" cat state, the probabilities of the cat being dead and alive are both $\frac{1}{2}$ and when we observe or measure his state the probabilities change to 0 (the state that is not observed) and 1 (the state that is observed).

This theory is associated with the scientists David Bohm and Louis de Broglie in what is called "Bohmian mechanics" or the "Broglie-Bohm Theory". In Bohmian mechanics a system of particles is described in part by its wave function, evolving, as usual, according to Schrödinger's equation. However, the wave function provides only a partial description of the system. This description is completed by the specification of the actual positions of the particles [4].

In Bohmian mechanics the state of a system composed of N particles is described by its wavefunction $\psi(q) = \psi(q_1, ..., q_N)$, a complex function on the space of possible configurations q of the system together with its actual configuration Q defined by the actual positions $Q_1, ..., Q_N$ of its particles [4]. To help us define this mechanics, we have two main equations, the traditional Schrödinger time evolution equation (2.7) and the "Guiding Equation" (2.8):

$$i\hbar\frac{\partial\psi}{\partial t} = H\psi \tag{2.7}$$

$$\frac{dQ_k}{dt} = \frac{\hbar}{m_k} Im\frac{\psi^*\partial_k\psi}{\psi^*\psi}(Q_1, ..., Q_N) \tag{2.8}$$

where m_k is the mass of the k-th particle, ∂_k is the gradient with respect to generic coordinates $q_k = (x_k, y_k, z_k)$ for the k-th particle. The right hand side of this last equation represents the probability current divided by the probability density ($\frac{J}{\rho}$).

As we can see, the two equations describing Bohmian Mechanics are very similar to the ones that are used in the orthodox interpretation of Quantum Mechanics and they give final results predicted by Quantum Mechanics experimentally. One of the interpretations that is different from the concept in the orthodox interpretation is the notion of collapse of the wavefunction: because of the incompleteness of Quantum Mechanics description and the need to consider the additional variables to fully describe a system, the measures on an observable just reveal pre existing states, so the wavefunction does not "collapse" in the way that it is interpreted as "forced to reduce its states to a well defined one".

2.4 Quantum Mechanics is complete

After this conceptions about the incompleteness of Quantum Mechanics, Everett and Wheeler proposed that Quantum Mechanics is a complete theory and their interpretation became known as "Many Worlds Interpretation". What gave this name to their theory is well exemplified by their explanation about the Schrödinger's Cat paradox: both accounts (alive and dead) are real, because each state represents a completely self-consistent account that can be real simultaneously when we consider more than a single world [2].

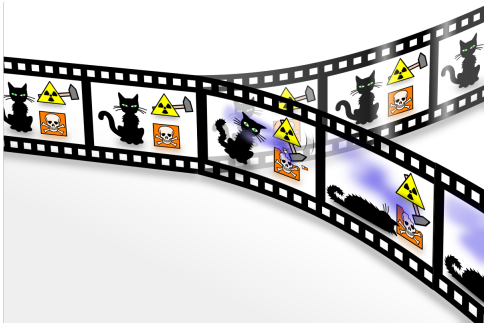

Figure 2.2: Schematic view of Schrödinger cat explanation by theory of Many Worlds Interpretation. Reference: [6]

To formalize this theory in mathematical ways, we can define $|s_i\rangle$ as a set of normalized states of a system S and $|d_i\rangle$ as a set of normalized states of a system D. If we suppose that the states of S and D are correlated, we can let D be a measuring device and take $|s_i\rangle$ as eigenstates of observables in system S. If the inital state of a measuring device is $|d_0\rangle$ and we define $|d_i\rangle$ as the measuring device indicating that the system S is in the state $|s_i\rangle$, we get this relation:

$$|s_i, d_0\rangle \rightarrow |s_i, d_i\rangle \tag{2.9}$$

In general S is in a superposition of states, so unitary time evolution during the measurement leads

to a final state in a superposition too, so we cannot define a state for S or D alone, just the relative states to each other.

$$\sum_i c_i \left|s_i, d_0\right\rangle \rightarrow \sum_i c_i \left|s_i, d_i\right\rangle \tag{2.10}$$

If we consider a index number m of identical systems $S^{(1)}, S^{(2)}, ...$ and n a index number of identical measuring devices of D, we get:

$$\left|s_i^{(m)}, d_0^{(n)}\right\rangle \rightarrow \left|s_i^{(m)}, d_i^{(n)}\right\rangle \tag{2.11}$$

Two measuring devices, $D^{(1)}$ and $D^{(2)}$ measure the same observable on a system S, first $D^{(1)}$ and then $D^{(2)}$. The evolution is described by:

$$\begin{aligned}\sum_i c_i \left|s_i, d_0^{(1)}, d_0^{(2)}\right\rangle &\rightarrow \sum_i c_i \left|s_i, d_i^{(1)}, d_0^{(2)}\right\rangle \\ &\rightarrow \sum_i c_i \left|s_i, d_i^{(1)}, d_i^{(2)}\right\rangle\end{aligned} \tag{2.12}$$

We can see that the two measuring devices always agree and, in general, any number of measuring devices measuring the same observable on the system S would always agree that S is in the state $|s_i\rangle$, i.e, relative to the state $|s_i\rangle$, measuring devices agree on an account for each i and according to the Many Worlds Interpretation each of these accounts are real.

If all the accounts are real, what do the coefficients c_i represent?

If we assume that a measuring device D measure the same observable in many identical systems prepared in the same initial state we can extend our notation and write:

$$\sum_{ij...} c_i c_j ... \left|s_i^{(1)}, s_j^{(2)}, ..., d_0\right\rangle \rightarrow \sum_{ij...} c_i c_j ... \left|s_i^{(1)}, s_j^{(2)}, ..., d_{ij...}\right\rangle \tag{2.13}$$

The right side in equation 2.13 is a superposition of terms representing all the systems $S^{(m)}$ in definite states with the measuring device indicating those. Each term corresponds to a definite account of the measurement and they are incompatible with all the other accounts.

The square of the absolute value of the coefficients in equation 2.13, according to the conventional interpretation of Quantum Mechanics represents the probability that the system $S^{(1)}$ is in the state $|s_i^{(1)}\rangle$, $S^{(2)}$ is in the state $|s_j^{(2)}\rangle$ and so on, but what this coefficients means if there is no collapse?

To answer this question, Everett interpreted equation 2.13 as a measure of the account that has $S^{(1)}$ in the state $|s_i^{(1)}\rangle$, $S^{(2)}$ is in the state $|s_j^{(2)}\rangle$ and so on, so the correspondence between worlds and accounts is not one-to-one, but many-to-one [2]. The measure makes the link between coefficients c_1, c_2,... to probabilities $|c_1|^2$, $|c_2|^2$,... of the final states.

To summarize it, if the probabilities of events $E_1, E_2, E_3, ...$ are $p_1, p_2, p_3, ...$ respectively, then the probability of a sequence of uncorrelated events $E_i, E_j, E_k, ...$ is $p_i \cdot p_j \cdot p_k, ...$ In the scenario described by the systems S and D with coefficients $c_i, c_j, ..$, the sequence of events has a measure $|c_i|^2 \cdot |c_j|^2 \cdot |c_k|^2, ...$ and if we randomly choose a world, the probability of this sequence equals its measure and the probability that a measurement on a system $S^{(m)}$ yield $|s_i^{(m)}\rangle$ in that world is $|c_i|^2$, just as the conventional interpretation predicts.

In conclusion, the Many Worlds Interpretation implies that Quantum Mechanics is complete and does not need a theory for collapse of the states, so we can use this explanation in the case of the cat paradox using this interpretation.

2.5 Conclusion

This work's intention was to show that Schrödinger's cat paradox has a much deeper interpretation that just "a superposition of states in which the cat is both alive and dad". All of the discussions were based on the initial problem: How can we explain the thought experiment of the cat in the box, and other ones like a pointer in orthogonal states, since in practical experience we always see a single state and not a superposition like the time evolution equations of Quantum Mechanics predicts?

A large number of theories were developed in an attempt to prove or disprove the completeness of Quantum Mechanics, involving other postulates like the collapse of the wavefuncition. All of theses theories are somehow giving an explanation for the Schrödinger cat, but many questions are still open for another discussions: How can we define collapse? Do systems have pre existing states and do we just measure them to reveal it or our observations (or consciousness) in fact produce the state? How can we "access" other worlds and demonstrate concretely that multiple exclusive accounts are all real?

Despite the fact that the experimental thought of Schrödinger cat was considered absurd even by its creator, we still hear a lot expressions like "Schrödinger cat states" even nowadays. Initially, the cat was a symbol of an impossibility or even

a detection of a flaw in Quantum Mechanics theory, but moderns cats ressignified this symbol and today we can actually observe and generate (even for macroscopic systems) entangled states or coherent superposition of states, named "Schrödinger cat states" [5].

In conclusion, we can say for sure that this paradox is still alive and open for new discussions. Schrödinger cat went from an absurdity and a challenge for the interpretations of Quantum Mechanics to a ressignified concept that is useful in many researches nowadays, characterizing systems with entangled states.

Bibliografia

[1] Franck Laloe. *Do We Really Understand Quantum Mechanics?*. 1 ed., 2012.

[2] Yakir Aharonov, Daniel Rohrlich. *Quantum Paradoxes: Quantum Theory for the Perplexed, Wiley*. 1 ed., 2004.

[3] Jean Bricmont. *Quantum Sense and Nonsense*. 1 ed., 2017.

[4] Sheldon Goldstein. *Bohmian Mechanics, The Stanford Encyclopedia of Philosophy*. Fall 2021 Edition, 2021.

Avaible on: `https://plato.stanford.edu/archives/fall2021/entries/qm-bohm/`

[5] Biao Xiong, Xun Li, Shi-Lei Chao, Zhen Yang, Wen-Zhao Zhang, Lin Zhou. *Generation of entangled Schrödinger cat state of two macroscopic mirrors*. Optics Express, 2019.

[6] `https://en.wikipedia.org/wiki/Many-worlds_interpretation`.

[7] `https://www.motherjones.com/kevin-drum/2018/09/schrodingers-cat-is-alive-one-twelfth-of-the-time/`.

[8] Bernard d'Espagnat. *On Physics and Phyilosophy*. Princeton University Press, 2006.

3

Rydberg atoms

Eliel Leandro Alves Junior
Instituto de Física de São Carlos, Universidade de São Paulo, 13560-970 São Carlos, SP, Brazil

Abstract: Um átomo de Rydberg é um átomo excitado para um nível de energia elevado, no qual atribuem algumas propriedades interessantes se comparados ao estado fundamental. Podemos destacar algumas dessas propriedades como uma forte interação dipolo-dipolo entre átomos de Rydberg próximos, grandes tempos de vida na ordem de microsegundos, a interação térmica diminui com o aumento do número quântico principal, utilização em computação e informação quântica, etc. Neste trablaho, propomos uma revisão teórica e uma aplicação desse átomo.

3.1 Introdução

Átomos de Rydberg foi descoberto pelo físico sueco Johannes Rydberg (1854-1919) por ter estudado as linhas espectrais e transações atômicas do átomo de Hidrogênio e forneceu muitas ferramentas para o estudo fundamental da matéria, e dentre elas, podemos destacar: propriedades e interações atômicas, coliões e transferência de energia, e utilização na computação e informação quântico. Os átomos de Rydberg podem ser qualquer átomo que são excitado para um nível de energia alto. O fato é saber em qual nivel de energia poderia chegar. No entanto, tem estudados recente de excitação experimental, que atingiram estados cujo o n está em torno de 200 e em algumas observações atronômicas existe evidências de estados na mesma ordem em estrelas.

A série de Rydberg foi descoberta como uma explicação empírica para as linhas espectrais do hidrogênio atômico e permitiu que a energia de ligação fosse expressa como:

$$E = -\frac{R_y}{n^2}. \tag{3.1}$$

onde R_y é um parâmetro de ajuste e n é um número inteiro. Pouco tempo depois, o desenvolvimento do modelo de Bohr mostrou que R_y não era apenas um parâmetro de ajuste, mas poderia ser calculado a partir de constantes fundamentais:

$$R_y = Z^2 \frac{m_e e^4}{8\epsilon_0^2 \hbar^2}. \tag{3.2}$$

3.2 Teoria

Átomos de Rydberg, a princípio, pode ser qualquer elemento da tabela periódica, porém são usados elementos da família $1A$ da tabela periódica, os alcalinos, pois apresentam um único elétron na cama de valência e se acemelham ao átomo de Hidrogênio, e por uma questão tecnológica são facilmente manipuláveis por lasers disponíveis atualmente, então, podemos escrever a equação de Schrodinger:

$$\left(-\frac{1}{2\mu} \bigtriangledown^2 + V(r)\right) \Psi(r,\theta,\phi) = E\Psi(r,\theta,\phi). \tag{3.3}$$

onde μ é a massa reduzida do elétron, $V(r) = -Z\frac{e^2}{4\pi\epsilon)0r}$ e r, θ e ϕ são as coordenadas esféricas. Considerando que não exista nenhuma força externa a equação (3.3) pode ser resolvida por separação de variáveis da seguinte forma:

$$\Psi(r,\theta,\phi) = R(r)Y_l^m(\theta,\phi). \tag{3.4}$$

onde $Y_l^m(\theta,\phi)$ são os harmônicos esféricos que depende apenas do momento angular do estado de Rydberg e a projeção ao longo do eixo de quantização m e $R(r)$ é a função radial. Portanto, substituindo a equação 3.4 na equação 3.3, podemos encontrar toda informação sobre a coordenada angular e radial da partícula. A solução da parte radial é dada por:

$$R_{n,l} = -\frac{(nl-1)!}{\sqrt{(n+1)!^3 2n}}\zeta^{3/2}e^{-\zeta r}(\zeta r)^l L_{n+1}^{2l+1}(\zeta r). \tag{3.5}$$

onde n é o número quântico principal, $\zeta = 2Z/n$ e L_{n+1}^{2l+1} os polinômios de Laguerre. A solução para a equação angular é dada por:

$$Y_l^m = \sqrt{\frac{(2l+1)(l-m)!}{4\pi(l+m)!}}P_l^m(cos(\theta))e^{im\phi}. \tag{3.6}$$

onde l é o número quântico relacionado ao momento angular orbital, m o número quântico relacionado ao campo magnético e P_l^m os polinômios de Legendre. Logo, encontramos a descrição completa de um estado ayômico para o átomo de Hidrogênio. É fundamental ressaltar que ao reescrevermos as equações utilizando a equação 3.4, a componente radial incorpora todas as informações do potencial, o qual, devido à separação de variáveis e ao sistema de coordenadas adotado, se torna um potencial efetivo que depende do número quântico l, de acordo com:

$$V_{eff} = \frac{\hbar^2 l(l+1)}{2\mu^2} - Z\frac{e^2}{4\pi\epsilon_0 r}. \tag{3.7}$$

Que incorpora o termo eletrostático, que naturalmente é atrativo, além de um termo centrífugo repulsivo, que depende do momento angular l. Ao conhecer o novo potencial e as funções de onda, podemos, por fim, determinar as autoenergias do elétron da seguinte maneira:

$$E_n = -\frac{\mu e^4 Z^2}{2\hbar^2(4\pi\epsilon_0)^2}\frac{1}{n^2}. \tag{3.8}$$

Esse resultado do átomo de hidrogênio é de extrema importância, pois nos auxilia a compreender a descrição dos átomos de Rydberg, os quais podem ser facilmente tratados como átomos hidrogenoides. A relação matemática entre eles e o Hidrogênio é conhecida como "defeito quântico" 3.2.2. Essa grandeza está relacionada com a interação do elétron mais externo com a nuvem eletrônica (que não existe no átomo de hidrogênio), a qual protege o núcleo positivo, resultando em uma diferença de fase entre as funções de onda do hidrogênio e as do átomo de Rydberg.

3.2.1 Funções de onda de Rydberg

Para obter as funções de onda dos átomos distintos do Hidrogênio em estados de Rydberg, é necessário a utilização de métodos numéricos, uma vez que a solução analítica se torna viável devido à complexidade do potencial e ao número de partículas envolvidas. Em especial, para o Rb^{85}, é utilizado o algoritimo conhecido como Numerov, que foi incorporado em um programa computacional gratuito denominado Radial [2]. A Figura 3.1 exibe, na subfigura (a), uma imagem comparativa entre o átomo de hidrogênio (H) e um átomo de Rydberg de Rubídio (Rb), juntamente com as funções de onda radial R(r) dos dois átomos. Nas subfiguras (b) e (c), respectivamente, são apresentadas as funções de onda radial R(r) para o mesmo estado eletrônico. $|50S_{1/2}\rangle$.

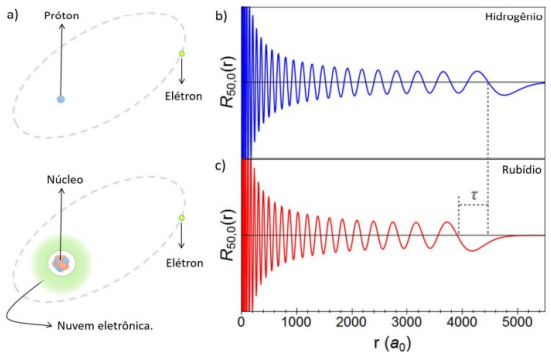

Figure 3.1: Função de onda radial para o estado $|50S_{1/2}\rangle$. Fonte:[2]

A Figura 3.2 (a), é exibido um gráfico comparativo entre o potencial efetivo de um átomo de Hidrogênio e o potencial modificado (51) (b), ambos para l = 0, utilizados no cálculo das funções de onda para os estados de Rydberg do Rb^{85}.

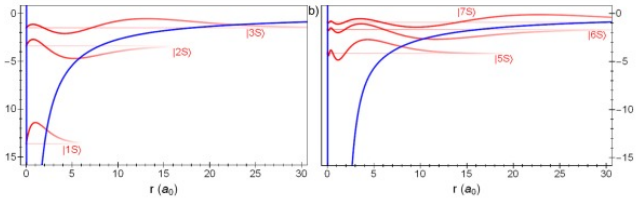

Figure 3.2: Comparação entre os potênciais atômicos do $Rb^{85}(b)$ e H (a). Fonte:[2]

Como resultado da interação entre o elétron e a nuvem eletrônica, também há uma alteração nos níveis de energia dos átomos. Essa modificação está diretamente ligada ao defeito quântico (3.2.2), que por sua vez é dependente do momento angular l do estado em consideração.

3.2.2 "Defeito Quântico"

Os átomos de metais alcalinos são semelhantes ao hidrogênio; um único elétron de valência orbita o núcleo em um potencial Coulombiano $1/r$. Entretanto, ao contrário do átomo de hidrogênio, muitos mais elétrons também orbitam o núcleo em raios mais curtos; como resultado, o elétron mais externo geralmente vê uma carga nuclear blindada. Estados de baixo momento angular ($l < 4$) desviam ainda mais do modelo hidrogenoide simples: a órbita do elétron de valência é altamente elíptica e pode penetrar nas camadas internas de elétrons. O elétron de valência está exposto à carga nuclear não blindada de um lado e à repulsão Coulombiana dos elétrons internos do outro lado, experimentando um potencial do núcleo muito diferente em distâncias curtas. Ao mesmo tempo, os elétrons de camada fechada podem ser polarizados pela presença do elétron de valência. Esses dois efeitos combinados aumentam a energia de ligação dos estados de Rydberg de baixo l, em relação aos estados hidrogenoides correspondentes. A energia de ligação dos metais alcalinos pode ser expressa como:

$$E = -\frac{R_y}{(n-\delta_{nlj})^2}, \tag{3.9}$$

onde δ_{nlj} é o defeito quântico. Agora podemos escrever um número quântico principal efetivo como $n^{'} = n - \delta_{nlj}$ para os estados de Rydberg de metais alcalinos. Os valores dos diferentes defeitos quânticos para Rb foram obtidos por meio de medições espectroscópicas [2] e podem ser calculados através da fórmula:

$$\delta_{nlj} = \delta_0 + \frac{\delta_2}{(n-\delta_0)^2} + \frac{\delta_4}{(n-\delta_0)^4} + ... \frac{3}{4}\alpha_c l^5. \tag{3.10}$$

sendo δ_i depende tanto de l quanto de j e α_c é uma correção devido à polarizabilidade do núcleo atômico para $l \geq 5$.

Estado	δ_0	δ_2
$\|nS_{1/2}\rangle$	3,13118	0,17
$\|nP_{1/2}\rangle$	2,65488	0,29
$\|nP_{3/2}\rangle$	2,64167	0,295
$\|nD_{3/2}\rangle$	1,34809	-0,6286

Table 3.1: Valores dos parâmetros δ_0 e δ_2. Fonte:[2]

Ao ter conhecimento do defeito quântico da espécie atômica em questão, é possível obter as energias de todos os estados aplicando alguns dados da Tabela **??** na Equação 3.10 e posteriormente na Equação 3.9. A Figura 3.3 ilustra um diagrama de energia que permite a comparação das energias entre diferentes estados n, lej do Rb^{85}. A última coluna representa os níveis energéticos do átomo de Hidrogênio para fins de comparação.

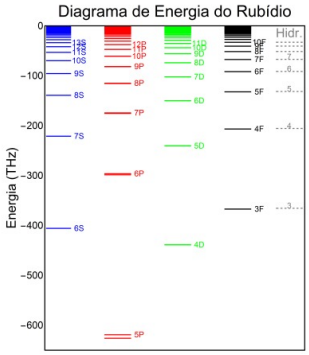

Figure 3.3: Diagrama de energia para o Rb^{85}. Fonte:[2]

Usando a teoria do defeito quântico, é possível encontrar outras características importes como o tempo de vida, energia de ligação do elétron, campo elétrico de ionização, raio orbital, momento de dipolo, polarizabilidade. A tabela **??** mostra os fatores das principais propriedades dos estados de Rydberg.

Propriedade	$n^* = n - \delta_{nlj}$
Energia de ligação do elétron	n^{*-2}
Compo elétrico de ionização	n^{*-4}
Raio da órbira	n^{*2}
Momento de dipolo	n^{*2}
Tempo de vida	n^{*3}
Polarizabilidade	n^{*7}

Table 3.2: Propriedades dos estados de Rydberg com o número principal quântico efetivo. Fonte:[2]

3.3 Propriedades

3.3.1 Raio atômico

O raio atômico r_{at}, é facilmente determinado, encontrando a posição de maior probabilidade na função de onda radial $|R(r)|^2$. Sabendo o raio atômico, a seção de choque geométrica pode ser encontrada diretamente da seguinte maneira $\sigma = \pi r^2$.

3.3.2 Polarizabilidade

Também podemos calcular a polarizabilidade, e pode ser obtido pela função de onda total, através do momento de dipolo das transições atômicas que pode ser calculado da seguinte maneira:

$$\langle n^{'}, l^{'}, j^{'} | (e\vec{r}) | n, l, j \rangle = e \int \psi_{n^{'},l^{'},j^{'}}(r,\theta,\phi)^{\dagger} \vec{r} \psi_{n,l,j}(r,\theta,\phi) d^3\vec{r} \tag{3.11}$$

Encontrando o momento de dipolo, podemos encontrar a polarizabilidade de um estado. A polarizabilidade α_s de um estado qualquer é dado por:

$$\alpha_s(n,l,j) = 2 \sum_{n^{'},l^{'},j^{'} \neq n,l,j}^{base} \frac{|\langle n^{'}, l^{'}, j^{'} | (e\vec{r}) | n, l, j \rangle|^2}{E_{n,l,j} - E_{n^{'},l^{'},j^{'}}} \tag{3.12}$$

sendo $E_{n,l,j}$ é a energia do estado $|n,l,j\rangle$. Na figura 3.4 (a), é apresentado um gráfico com o cálculo do momento de dipolo via equação 3.11 entre o primeiro estado excitado $5P_{3/2}$, para outros estados de Rydberg. Em (b) apresenta o cálculo da polarizabilidade.

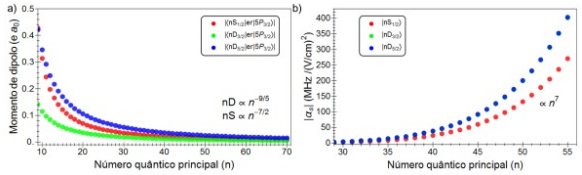

Figure 3.4: Momento de dipolo e polarizabilidade. Fonte:[2]

3.3.3 Interações de longo alcance dos átomos de Rydberg

As interações de longo alcance são conhecidas como alterações nos níveis atômicos devido à proximidade de outros átomos. Essas interações ocorrem devido à sensibilidade dos átomos ao ambiente externo, como sua alta polarizabilidade discutida anteriormente. Para as interações de longo alcance, os átomos de Rydberg são tratados como dipolos elétricos. Essa interação entre os átomos pode ser descrita como uma interação clássica entre dois dipolos, $\vec{p}_1$ e $\vec{p}_2$ e a formula é escrita abaixo:

$$V_{dd}(\vec{R}) = \frac{\vec{p}_1 \cdot \vec{p}_2}{|\vec{R}|^3} - 3\frac{(\vec{p}_1 \cdot \vec{R})(\vec{p}_2 \cdot \vec{R})}{|\vec{R}|^5}, \tag{3.13}$$

onde $\vec{R}$ é o vetor> Agora considerando a interação não clássico, o dipolo elétrico pode ser escrito como um momento de dipolo de transição entre os estado ψ e $\psi^{'}$. então, $\vec{p} = \langle\psi| e\vec{r} |\psi^{'}\rangle$. Logo, o potencial é dado por:

$$V_{dd}(\vec{R}) \propto \frac{1}{|\vec{R}|^3} \sum_{ij} \sum_{kl} \langle\psi_i| e\vec{r} |\psi_j^{'}\rangle \langle\psi_k| e\vec{r} |\psi_l^{'}\rangle . \tag{3.14}$$

onde os índices i e j representam o estados do átomo 1 e os índices k e l os estados do átomo 2.

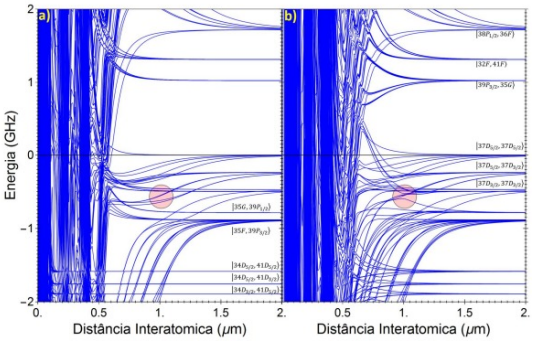

Figure 3.5: Figura (a) o potencial foi calculado considerando apenas a interação de dipolo-dipolo, e no da direita (b) considerando também dipolo-quadrupolo e quadrupolo-quadrupolo. Fonte:[2]

3.3.4 Efeito Stark

A alta polarizabilidade dos átomos de Rydberg faz com que eles sejam muito sensíveis a campos elétricos externos. Essa interação entre um átomo e um campo elétrico é conhecida como efeito Stark **??**. Uma das principais consequências dessa interação é a modificação dos níveis de energia internos do átomo, levando à quebra da degenerescência das projeções do momento angular |mji. Isso significa que os diferentes estados do átomo, que antes tinham a mesma energia, agora terão energias diferentes devido à presença do campo elétrico.

Na figura 3.6, são apresentados exemplos de cálculos do efeito Stark para estados próximos ao estado $50S_1/2$ nas subfiguras (a) e (b). A subfigura (c) mostra um mapa que ilustra os estados $37D_3/2$ e $37D_5/2$ em termos das regiões de campo e energia que podem ser experimentalmente acessadas.

Existe outras propriedades dos atómos de Rydberg como o tempo de vida entre outros, porém não será mencionadas neste trabalho. A próxima seção abordará uma aplicação dos atómos de Rydberg.

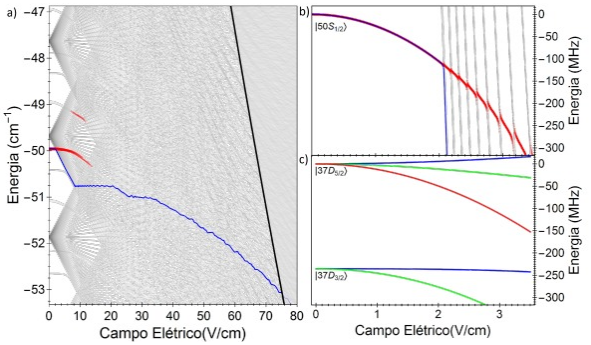

Figure 3.6: Efeito Stark. Fonte:[2]

3.4 Experimento

As interações entre átomos de Rydberg desempenham um papel importante na investigação de propriedades intrínsecas da matéria em baixas temperaturas. Essas interações são fundamentais para a compreensão de interações de longo alcance, colisões atômicas, formação de moléculas e também para a manifestação macroscópica de fenômenos atômicos, como as interações de van der Waals e dipolo-dipolo. Adicionalmente, as interações entre átomos de Rydberg são de extrema importância para impulsionar o avanço da computação quântica e outros estudos. Basicamente esses sistemas dependem do fenômeno de bloqueio dos átomos de Rydberg, que é uma limitação na densidade populacional desses átomos devido à forte interação entre eles. Porém, essas mesmas interações podem resultar na degradação da coerência em amostras atômicas. Essas interações podem trazer tanto benefícios quanto desafios em sistemas atômicos, portanto, é de extrema importância compreendê-las adequadamente.

O experimento realizado por [1], estuda a anisotropiia da interação dipolo-dipolo, e portanto, compreendendo o efeito de bloqueio de Rydberg especificamente em uma amostra atômica confinada e mantida em uma armadilha óptica de dipolo tipo QUEST. O experimento começa utilizando uma armadilha magnética ótica (MOT) que é utilizada para carregar a armadilha QUEST, assim produzindo uma amostra atômica de 10^6 átomos como uma densidade de $10^12 tomos/cm^3$. Toda informação sobre a configuração experimental pode ser encontradas em [3,4]. Para excitar o estado $50S - 1/2$ é utilizado pulsos de laser [1]. Todos os campos elétricos utilizados são gerados por um sistema de 8 eletrodos que são independentemente controlados, seguindo a seguinte configuração **??**. Os elétrons são detectados usando um detector de placa micronal(MCP), fornecendo assim uma média de 300 átomos de Rydberg.

Durante a sequência de pulsos de laser, a população atômica retida na QUEST diminui, permitindo a investigação da população do estado de Rydberg $50S_{1/2}$ em relação à densidade atômica do estado fundamental. Para analisar o decaimento da amostra, utilizou-se a técnica de imagem de absorção seletiva de estados. Então, para estados nS sem utilizar o campo elétrico, os átomos interagem apenas por meio da interação de van der Waals, de modo que o potencial é puramente repulsivo e isotrópico. Na presença de um campo externo,os átomos se polarizam e a interação muda para um potencial efetivo dependente do ângulo [1]. Este potencial. O primeiro resultado foi obter um espectro Stark. Na figura 3.7 (a) é mostrado uma população normalizada de $50S_{1/2}$ em função do campo contínuo $\Delta 480 = -151 MHz$ e combinando um espectro semelhante para diversos valores $\Delta 480$, obtem o espectro Stark 3.7(b)

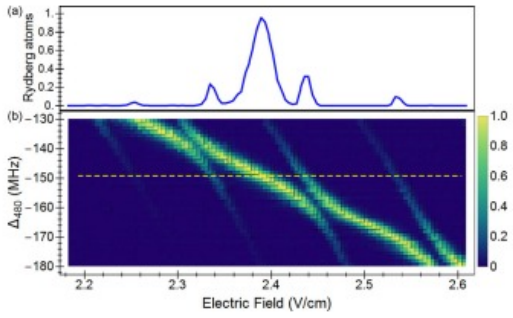

Figure 3.7: a) População no $50S_{1/2}$, b) Espectro Stark. Fonte:[2]

Os eletrodos utilizados foram calibrados por meio de vários mapas Stark próximos ao estado $50S_{1/2}$ e comparados com os valores teóricos em cada direção (X, Y e Z). Isso permitiu obter a posição de campo zero e o fator de calibração para cada coordenada. Antes de cada medição do bloqueio de Rydberg em um ângulo específico, foi realizada uma varredura do campo para verificar a posição da ressonância desejada. Ajustando o campo nessa ressonância, a amplitude do campo foi garantida para todos os ângulos dentro de 20 $mVcm^-1$. Durante a variação do ângulo, pequenas variações nas voltagens aplicadas nos eletrodos foram feitas para manter a ressonância. Simulações computacionais indicaram que essas variações de voltagem resultaram em um erro angular inferior a 4.

A Figura 3.8, que apresenta um gráfico da população do estado 50S1/2 em relação à densidade dos

átomos no estado fundamental para diferentes orientações de campo. O campo aplicado possui uma amplitude de $2,38\ V\ cm^{-1}$ e $\Delta 480 = -151 MHz$.

Para comprovar a consistência dos resultados obtidos com o bloqueio de átomos de Rydberg, foi aplicado um modelo clássico de esferas rígidas no estado estacionário. Esse modelo é um dos mais simples disponíveis na literatura, porém, contém as principais informações físicas e descreve de forma adequada o efeito observado.

Para comparar a dependência angular experimental da população $50S_{1/2}$ com o modelo de esferas rígidas de bloqueio, plotamos o número médio final de átomos de Rydberg em função do ângulo do campo elétrico, como mostrado na Figura 3.9.

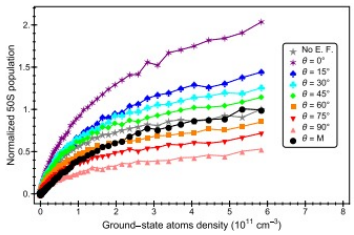

Figure 3.8: a) População no $50S_{1/2}$. Fonte:[2]

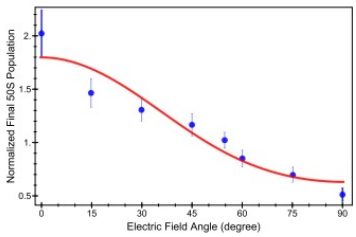

Figure 3.9: População do estado $50S_{1/2}$ em função do angulo. Fonte:[2]

Em outro experimento, foi realizado um estudo para explorar a capacidade de anular as interações dipolo-dipolo. A população do estado $50S_{1/2}$ foi medida em relação à densidade atômica do estado fundamental para diferentes campos elétricos no ângulo mágico. As amplitudes dos campos elétricos foram escolhidas de forma a evitar cruzamentos entre o estado $50S_{1/2}$ e as linhas hidrogênicas do manifol. Diferentes amplitudes de campo resultam em uma mudança na força de interação e, consequentemente, na população final de átomos de Rydberg. No entanto, como foi demonstrado anteriormente, no ângulo mágico, a interação dipolo-dipolo é suprimida, o que implica que as curvas de população devem ser independentes da amplitude do campo. Esse comportamento pode ser observado na Figura 3.10.

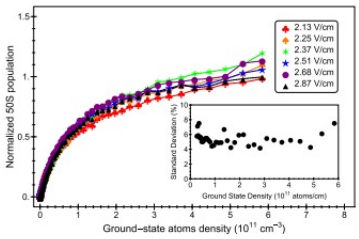

Figure 3.10: A população do estado $50S_{1/2}$ em função da densidade dos átomos no estado fundamental em função do campo. Fonte:[2]

3.5 Conclusão

Mostramos que os átomos de Rydberg possuem algumas propriedades como uma forte interação dipolo-dipolo entre átomos de Rydberg próximos, grandes tempos de vida na ordem de microsegundos, a interação térmica diminui com o aumento do número quântico principal, utilização em computação e informação quântica, etc. Na seção 3.4 apresentamos alguns resultados do experimento feito por [1]. Podemos chegar a seguinte conclusão, a interação entre dois átomos de Rydberg é mais intricada do que o potencial simplificado com base no parâmetro de interação derivado do efeito Stark em átomos individuais. Esse potencial simplificado é válido apenas em distâncias longas e não no regime de bloqueio. Em um estudo recente, foi comprovado que o caráter multinível da interação, devido à presença de estados de momento angular elevado, é crucial para calcular curvas de potencial precisas e interpretar experimentos de interação de Rydberg. E o modelo de bloqueio de esferas rígidas é bastante simplificado e não coincide com os resultados experimentais em densidades mais elevadas. Em um estudo anterior, foi observado que, mesmo quando o modelo de bloqueio atinge sua saturação em altas densidades, a população de átomos de Rydberg medida experimentalmente continua a aumentar gradualmente.

Bibliografia

[1] GONÇALVES, L. F.; MARCASSA, L. G. *Physical Review A, v. 94, p. 043424 2016.*

[2] GONÇALVES, L. F. *Interações entre átomos de Rydberg no regime de bloqueio de excitação,*

2016, Tese Doutorado em Física, Universidade de São Paulo, São Carlos, 2016.

[3] J. M. Kondo, L. F. Gonc¸alves, J. S. Cabral, J. Tallant, and L. G. Marcassa. *Phys. Rev. A 90, 023413 2014.*

[4] J. M. Kondo, D. Booth, L. F. Gonc¸alves, J. P. Shaffer, and L. G. Marcassa, *Phys. Rev. A 93, 012703 2016.*

4

The quantum jump, its history and observation

Gabriel de Oliveira Campos

Instituto de Física de São Carlos, Universidade de São Paulo, 13560-970 São Carlos, SP, Brazil

Abstract: Formulado em 1913 por Niels Bohr, o conceito de salto quântico surgiu para identificar as transições descontínuas dos elétrons entre níveis energéticos atômicos e tornou-se foi alvo de intensa discussão entre duas das principais vertentes de pensamento da mecânica quântica. Tal fenômeno teve sua primeira observação experimental em 1986, através da espectroscopia de um único íon, demonstrando alta concordância com as ideias teóricas propostas por Bohr. Apesar de vários outros experimentos posteriores à 1986 também fornecerem resultados discretos para as transições, o presente texto buscará expor as diferentes interpretações ao longo da história, bem como tratamentos numéricos computacionais para tal fenômeno, permitindo a formação de uma visão mais generalista sobre um assunto de nível tão fundamental dentro da física.

4.1 Introdução

O desenvolvimento da Mecânica Quântica no século XX e seus inúmeros efeitos, propiciaram uma revolução na compreensão sobre os processos de medição. Em particular duas vertentes de pensamento ganharam alta relevância dentro desse cenário: uma com visão puramente probabilística ("interpretação de Copenhague") - desenvolvida por Niels Bohr e Werner Heisenberg - e outra seguindo o caminho da mecânica ondulatória, apoiada por Erwin Schrödinger e Albert Einstein.

Uma das mais intensas discussões entre as duas interpretações surgiu em razão da proposta de Bohr para as transições entre níveis energéticos atômicos. Em sua análise, tais processos aconteceriam de forma instantânea e probabilística através dos denominados saltos quânticos, indo totalmente na contramão das ideias ondulatórias - que defendiam a existência dos níveis energéticos em termos da superposição de modos vibracionais. Em meados de 1980, após o desenvolvimento dos lasers, detecções experimentais dos saltos quânticos foram conduzidas, demonstrando uma correlação quase direta entre os resultados e a interpretação de Bohr.

Nesse âmbito, considerando o caráter fundamental dos saltos quânticos e as divergências entre os dois tratamentos para a mecânica quântica, o presente trabalho buscará abordar a história desses eventos, os processos experimentais e teorias empregadas em suas primeiras medições e por fim, uma maneira intuitiva de simular computacionalmente os saltos quânticos para um sistema de dois níveis através do método de Monte Carlo, buscando adentrar em todas as etapas nos méritos de cada uma das interpretações.

4.2 Contexto histórico

O conceito de saltos quânticos surgiu com as análises de Niels Bohr sobre a estrutura atômica da matéria em 1913 [1]. Através de seus estudos sobre so espectros de emissão de determinados gases, Bohr concluiu que os elétrons de um átomo poderiam ocupar diferentes valores discretos de energia e, mediante a processos - absorção, emissão espontânea e emissão estimulada -, transitariam de forma abrupta entre esses níveis energéticos. Tais transições instantâneas foram denominadas saltos quânticos e pavimentaram caminho para intensos debates ao longo do século XX.

Com o desenvolvimento da mecânica quântica ondulatória, começaram a surgir questionamentos sobre o conceito dos saltos quânticos. A interpretação de Copenhague para a mecânica quântica, defendida por Bohr e Heisenberg, trazia aos saltos um

caráter aleatório e instantâneo, entrando em conflito as visões de físicos como Schrödinger e Einstein - que associavam ao fenômeno uma descrição para níveis energéticos dos elétrons em termos dos modos de vibração fundamentais [2]. Indo em contramão com as ideias de Schrödinger, o modelo proposto Bohr também não previa a possibilidade dos níveis de energia existirem como superposição coerente de estados, restringindo a ocorrência de saltos quânticos em sistemas cuja evolução temporal se desenvolvesse de tal forma e norteando uma evolução energética tal como exemplificado na **Fig. 4.1**.

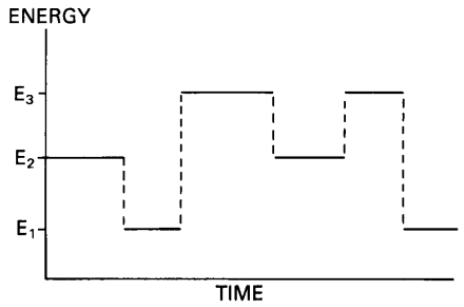

Figure 4.1: Evolução temporal da energia no modelo de Bohr - ilustração intuitiva para os saltos quânticos [3].

As discordâncias entre as visões geraram debates calorosos entre Bohr e Schrödinger evidenciados, por exemplo, pela seguinte declaração feita por Schrödinger: "If all this damned quantum jumping were really to stay, I should be sorry I ever got involved with quantum theory" [3] e a consequente resposta de Bohr: "But we others are very grateful to you that you did, since your work did so much to promote the theory".

Apesar da grande aceitação de inúmeras noções colocadas pela mecânica quântica ondulatória, o surgimento da tecnologia de captura de íons por Hans Dehmelt e colaboradores [5] e a observação da fluorescência induzida por laser em um único átomo possibilitaram uma interpretação quase direta em termos das visões de Bohr para os saltos quânticos. Nesse sentido, o tópico a seguir buscará discutir as primeiras observações desse fenômeno, a teoria por trás desse experimento e uma análise geral sobre seus resultados.

4.3 Observações experimentais

Atrelado ao desenvolvimento da técnica de captura de íons [5] - utilizando lasers sintonizados pouco abaixo da frequência de ressonância atômica e induzindo forças de radiação impedindo a translação do íon - as possibilidades de estudar espectroscopia em sistemas quase ideais foram atingidas, evitando distorções por desvio Doppler ou processos colisionais. Dentre os efeitos estudados nesses sistemas, a fluorescência telegráfica atômica ganhou enorme destaque, uma vez que permitiu avaliar a dinâmica transicional em um sistema quântico de três níveis e seus respectivos saltos.

4.3.1 O sistema de três níveis e a fluorescência telegráfica

Parte da relevância em estudar os sistemas de três níveis, encontra-se diretamente relacionado à teoria dos processos de medição dentro da mecânica quântica. Segundo John von Neumann [11], os processos de medida de um estado puro seguiriam dois passos: 1° - a projeção do operador do estado medido em termos dos autovetores da base do medidor e 2° - a observação de um dos possíveis autovalores do aparato de medição. A utilização de um sistema de três níveis possuindo uma transição fraca - representando a amostra - e uma forte - correspondendo ao medidor seria então uma forma simplificada de avaliar algumas das principais características desses processos de medição e será abordada exaustivamente ao longo do texto.

Consideremos um sistema quântico de três níveis em configuração V, tal como mostrado na **Fig. 4.2**, com uma transição forte (detector) e outra fraca (amostra) - por exemplo a transição dipolar $S_{1/2} - P_{1/2}$ e a transição quadripolar $S_{1/2} - D_{5/2}$ do íon de bário, respectivamente. Sob a incidência de radiação por um laser CW, ocorrem as possibilidades de transição entre níveis $0 \longleftrightarrow 1$ (forte) e $0 \longleftrightarrow 2$ (fraca), com alta prioridade para transição forte. Assumindo agora a existência de um segundo laser responsável por excitar as transições fracas, o sistema quântico irá preferencialmente realizar transições $0 \to 1 \to 0 \to 1 \to 0...$, podendo em algumas das excitações, transitar entre $0 \to 2$ e permanecer nesse estado com tempo de vida muito maior que os outros - denominado estado metaestável - até decair novamente para o estado fundamental.

Devido ao baixo tempo de vida (τ«1s) das transições fortes, todo processo de desexcitação ocorre muito rapidamente e a fluorescência coletada teria um sinal esperado praticamente contínuo. Entretanto, observa-se que a existência de um estado metaestável com tempo de vida muito maior que o tempo de vida da transição forte, permite um "arquivamento" do elétron no estado 2 - induzindo a

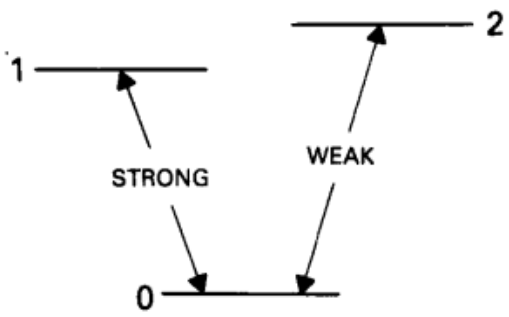

Figure 4.2: Estados energéticos para um sistema de três níveis com uma transição fraca e uma forte, configuração V [3].

manifestação de períodos de escuridão na detecção de fluorescência. Dessa maneira, são obtidos períodos luminosos intercalados de períodos aleatórios sem luz, característicos da fluorescência telegráfica, possibilitando a utilização desse sinal com um monitor direto para os saltos quânticos [3].

Vale ressaltar que, apesar de muito interessante, o processo citado anteriormente sofre ação de efeitos indesejados uma vez que, em razão dos dois lasers induzirem simultaneamente a transição fraca e forte, são produzidas perturbações na coerência da transição fraca - movida pela dinâmica das transições fortes. Uma solução para tal problema foi proposta por Dehmelt [11], idealizando o chamado amplificador quântico, que alternaria a irradiação do laser da amostra com o laser do detector, corrigindo esse problema.

4.3.2 Observando os saltos quânticos pela primeira vez

A primeira observação do fenômeno dos saltos quânticos foi realizada por Warren Nagourney, Jon Sandberg e Hans Dehmelt em 1986 [4], por meio da técnica de fluorescência telegráfica para um íon de Ba^+. Para melhor compreensão do experimento, consideremos o diagrama da **Fig. 4.3**, sob a incidência de um feixe laser, um íon de Ba^+ inicialmente no estado $5^2S_{1/2}$ pode migrar para $6^2P_{1/2}$, resultando na possibilidade de transição entre $6^2P_{1/2} \rightarrow 5^2S_{1/2}$ e $6^2P_{1/2} \rightarrow 5^2D_{3/2}$. Em virtude da alta taxa de decaimento para $5^2D_{3/2}$, faz se necessário o uso de um segundo laser excitando a transição $6^2P_{1/2} \rightarrow 5^2D_{3/2}$, impedindo que a fluorescência de ressonância seja desligada após a emissão de poucos fótons. Dessa forma, ambas transições são acionadas e observa-se uma forte emissão em 493.4 nm para $6^2P_{1/2} \rightarrow 5^2S_{1/2}$ e uma emissão mais fraca em 649.9 nm para $6^2P_{1/2} \rightarrow 5^2D_{3/2}$.

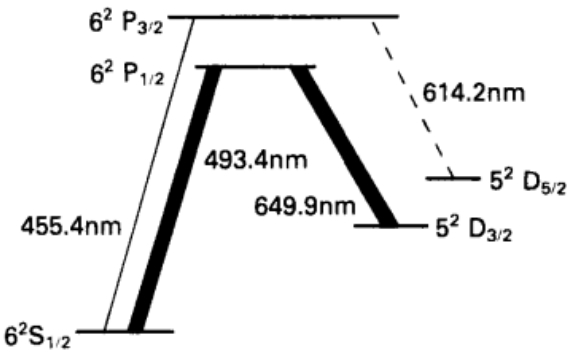

Figure 4.3: Diagrama de energia para o íon de Ba^+ utilizado na primeira detecção dos saltos quânticos [4].

Para ativação da fluorescência telegráfica, uma nova fonte de radiação deve ser colocada no sistema (no caso do experimento uma lâmpada de cátodo oco de bário), induzindo fracamente as transições entre $5^2S_{1/2} \rightarrow 6^2P_{3/2}$ e quebrando o ciclo $6^2P_{1/2} \rightarrow 5^2S_{1/2}, 5^2D_{3/2}$. Assim, quando excitado, o íon passa a produzir uma fluorescência em 455.4nm, resultante da transição $6^2P_{3/2} \rightarrow 5^2S_{1/2}$ podendo em, um instante aleatório, transitar do estado $6^2P_{3/2}$ para o estado metaestável $5^2D_{5/2}$ e permanecer lá em um tempo característico de cerca de 30s até saltar novamente para o estado $5^2S_{1/2}$. Tal processo de "arquivamento" do íon no estado metaestável, fornece ao experimento longos períodos sem nenhuma fluorescência e permite a observação direta da aparente descontinuidade entre saltos quânticos. A **Fig. 4.4** busca mostrar os resultados obtidos experimentalmente para a fluorescência telegráfica em 493.4nm.

Experimentalmente, um laser LD490 foi aplicado para excitar a linha de 493.4nm e um laser DCM para a linha de 649.9 nm do íon de Ba^+. Uma lâmpada de Bário induziu a emissão em 455.4 nm e um filtro de interferência fez a seleção dos comprimentos de onda de saída. Um gabinete de vácuo composto por um bloco de aço inoxidável com janelas, bomba e componentes eletrônicos foi utilizado para manter uma pressão de cerca de 8×10^{-11} Torr. Além disso, o íon de Ba^+ foi exposto ao campo magnético ambiente, sem a presença de bobinas ou blindagem magnética.

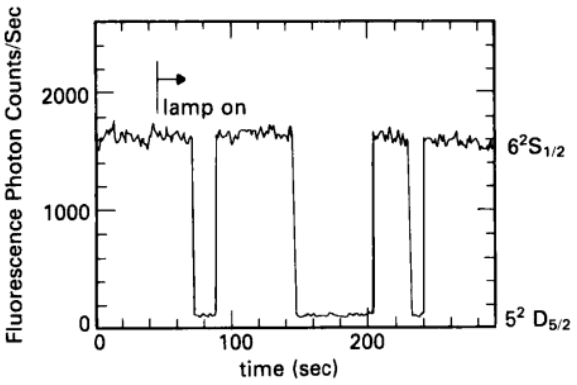

Figure 4.4: Medidas de fluorescência telegráfica para o íon de Ba^+ [4].

4.3.3 Outras observações

Mais experimentos de fluorescência telegráfica foram conduzidos em 1986 por Bergquist, Hulet, Itano e Wineland [6] - avaliando os períodos de "arquivamento" no estado metaestável $5d^9 6s^2\ ^2D_{5/2}$ de um íon de Hg^+- e por Sauter, Neuhauser, Blatt e Toschek [7] - novamente com o íon de Ba^+, porém sem excitar a transição $5^2S_{1/2} \rightarrow 6^2P_{3/2}$ e observando o arquivamento no estado metaestável $5^2D_{5/2}$ por espalhamento Raman-Stokes - ambos demonstrando uma alta correlação entre os resultados obtidos experimentalmente e a interpretação de Copenhague.

Historicamente, houve alguma resistência por parte dos autores que consideravam as ideias da mecânica quântica ondulatória para aceitar a explicação desse fenômeno de fluorescência telegráfica como manifestações dos saltos quânticos de Bohr, passando a questionar, em particular, a natureza da permanência nos estados metaestáveis [3].

Alguns autores [8], por sua vez, buscaram conciliar as duas visões para os saltos quânticos considerando que, para medições em um intervalo de tempo suficientemente pequeno, a superposição coerente de estados não se desenvolveria e seria válida - em boa aproximação - a descrição de Bohr. Tal argumento é sustentado pelo denominado efeito Zeno, observado experimentalmente em 1990 por Itano, Heizein, Bollinger e Wineland [9]. Simplificadamente, tal efeito pode ser compreendido assumindo a evolução temporal de um sistema quântico, dado na imagem de Schrödinger por:

$$|\psi\rangle = e^{-i\hat{H}t}|\psi_0\rangle \tag{4.1}$$

Com $\hbar = 1$. Nessa condição a probabilidade de encontrar o sistema no estado inicial em um intervalo δt valerá então:

$$\begin{aligned} P_0(\delta t) &= |\langle\psi_0|e^{-i\hat{H}t}|\psi_0\rangle|^2 \\ &= |\langle\psi_0|\psi_0\rangle - i\langle\hat{H}\rangle\delta t - \frac{(\delta t)^2\langle\hat{H}\rangle}{(2!)} + \mathcal{O}(\delta t^3)|^2 \\ &\approx 1 - \Delta H^2(\delta t)^2 \end{aligned} \tag{4.2}$$

Logo, para N medidas sucessivas e com intervalos temporais de (δt - t = nδt):

$$\begin{aligned} P_0(t) &= [1 - \Delta H^2(\delta t)^2]^N \\ &= [1 - \frac{\frac{t^2}{N}\Delta H^2}{N}]^N \\ &\approx e^{-\frac{t^2}{N}\Delta H^2} \end{aligned} \tag{4.3}$$

Através da Eq. 4.3, conclui-se que para muitas medidas ($N \rightarrow \infty$) a probabilidade do estado permanecer na mesma configuração tende à 1. Portanto, ocorre uma inibição da evolução temporal do sistema em uma superposição coerente de estados, favorecendo a interpretação dos saltos quânticos ao ângulo de Bohr.

4.4 Simulando saltos quânticos com Monte Carlo

A aplicação de métodos estocásticos, como Monte-Carlo Wave Function (MCWF), no estudo dos saltos quânticos data do início da década de 1990 [10]. Buscando vislumbrar uma pequena parte do poder desse método e fazer alguma conexão com a mecânica quântica ondulatória, imaginemos um sistema de dois níveis governado pela equação de Schrödinger e com Hamiltoniano dado por:

$$\hat{H} = \begin{pmatrix} 0 & \frac{\hbar\Omega}{2} \\ \frac{\hbar\Omega}{2} & -\hbar\Delta \end{pmatrix} \tag{4.4}$$

Sendo $\Delta = \omega - \omega_0$ a dessintonização entre a frequência da luz e a frequência da transição e Ω a frequência de Rabi. Evoluindo o sistema temporalmente, considerando que a função de onda se encontra em uma superposição de estados dada por $|\Psi(t)\rangle = c_1|1\rangle + c_2|2\rangle$ e que o sistema em t=0 encontra-se no estado fundamental $|\Psi(0)\rangle = |1\rangle$, torna-se possível determinar as probabilidades de encontrar o átomo em cada um dos estados através de:

$$P_1(t) = |\langle 1|\Psi(t)|1\rangle|^2 = |c_1(t)|^2 = cos^2\frac{\Omega t}{2} \quad (4.5)$$

$$P_2(t) = |\langle 2|\Psi(t)|2\rangle|^2 = |c_2(t)|^2 = sin^2\frac{\Omega t}{2} \quad (4.6)$$

Nesse sentido, como tratado em [10], a construção de um código para avaliar os processos de emissão estimulada e absorção pode ser elaborada subdividindo o tempo de observação dos estados em intervalos do tipo $T_n = n\Delta t$ (com n = 0,1,2...), gerando números aleatórios r_n entre [0,1] e assumindo condições para possíveis transições entre os estados $|1\rangle$ e $|2\rangle$ dadas via $P_2(t)$(uma vez que $P_1(t) = 1 - P_2(t)$), então se:

1. $P_2(t_{n-1}) < r_{n-1}$e $P_2(t_n) < r_n \Rightarrow |\Psi\rangle = |1\rangle$
2. $P_2(t_{n-1}) < r_{n-1}$e $P_2(t_n) \geq r_n \Rightarrow |\Psi\rangle = |2\rangle$
3. $P_2(t_{n-1}) \geq r_{n-1}$e $P_2(t_n) \geq r_n \Rightarrow |\Psi\rangle = |2\rangle$
4. $P_2(t_{n-1}) \geq r_{n-1}$e $P_2(t_n) < r_n \Rightarrow |\Psi\rangle = |1\rangle$

Em 2 e 4 temos respectivamente os processos de absorção e emissão estimulada, sendo as condições de alteração imediata entre estados $|1\rangle$ e $|2\rangle$ características dos saltos quânticos. Na **Fig. 4.5** encontram-se algumas trajetórias quânticas - sendo uma média sobre uma série de N medições - simuladas em [10] - para 1, 10, 100, 10^5 átomos - com os valores de $\Omega = 5 \times 10^4$ Hz e $\Delta t = 10^7 s$ e N = 100, demonstrando o comportamento em termos dos saltos quânticos discretos para 1 átomo e o caráter oscilatório para sistemas com mais átomos, assim como esperado para uma simulação estocástica.

Para a completeza da análise, uma construção similar com MCWF pode ser realizado para a emissão espontânea em um sistema de dois níveis [11], assumindo a existência de um termo dissipativo para energia dentro do hamiltoniano efetivo, tal como:

$$\hat{H}_{eff} = \begin{pmatrix} 0 & \Omega \\ \Omega & \Delta - \frac{i\Gamma}{2} \end{pmatrix} \quad (4.7)$$

A sutiliza entre considerar ou não a emissão espontânea encontra-se na diculdade que o hamiltoniano exposto em 4.7 adiciona à simulação. A presença do termo imáginário na diagonal principal torna esse operador não hermitiano ($[\hat{H}_{eff}, \hat{H}^{\dagger}_{eff}] \neq 0$) e produz uma necessidade de renormalização do sistema já que:

$$\langle\psi|\psi\rangle \rightarrow e^{-\Gamma t} \quad (4.8)$$

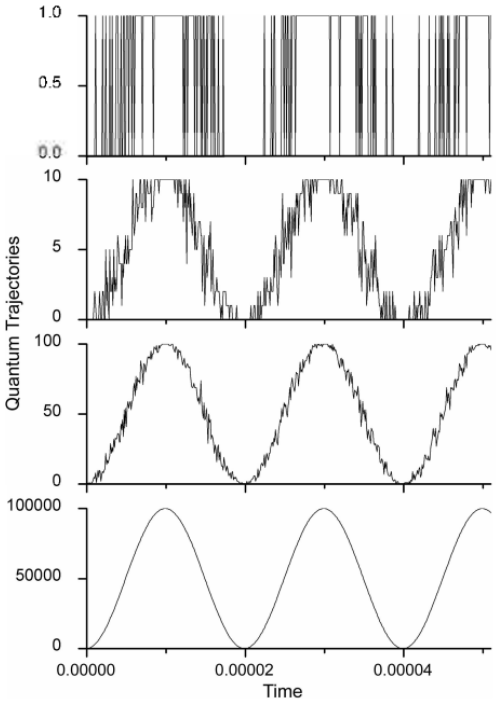

Figure 4.5: Simulação para a trajetória dos saltos quânticos considerando absorção e emissão estimulada em um sistema de dois níveis. Os gráficos demonstram, respectivamente, o número de 1, 10, 100 e 10^5 átomos simulados [10].

Nesse âmbito, um código para avaliar o processo de emissão espontânea pode ser construído considerando que, para $r_n > 1 - \langle\psi|\psi\rangle$, o sistema não possuirá dissipação e sofrerá apenas uma renormalização junto à sua evolução temporal e, se $r_n < 1 - \langle\psi|\psi\rangle$ haverá dissipação e o sistema retornará para o estado fundamental $|\psi_0\rangle$ [11]. As condições citadas se encontram abaixo em 1 e 2, respectivamente.

1. $\frac{(1-i\hat{H}dt)|\psi(t+dt)\rangle}{\sqrt{\langle\psi(t)|\psi(t)\rangle}}$ para $r_n > 1 - \langle\psi|\psi\rangle$
2. $|\psi_0\rangle$ para $r_n < 1 - \langle\psi|\psi\rangle$

A **Fig. 4.6** busca demonstrar os resultados obtidos para simulação do sistema considerando a emissão espontânea e os seguintes parâmetros $\Omega = 60\pi \times 10^6$Hz, $\Delta = 30\pi \times 10^6$Hz, $\Gamma = 12\pi \times 10^6$ e $dt = 0.5 \times 10^{-9} s$. Os saltos quãnticos são avaliados considerando a função de onda no estado fundamental, correspondente aos processos de fluorescência analisados experimentalmente. Observa-se então, além de uma modificação da função de onda $|\psi(t)\rangle$ pela não observação da emissão espontânea -

reduzindo a população do estado excitado em $1-\Gamma dt$ [11], a presença de oscilações para os valores médios de população a medida que o tempo progride. Tais resultados obtidos através das simulações com MCFW, além de abrirem espaço para estudos computacionais da estatística de fenômenos que até o momento não possuem unanimidade nas discussões analíticas, pavimentam caminho para predição do comportamento dos saltos quânticos em sistemas mais complexos.

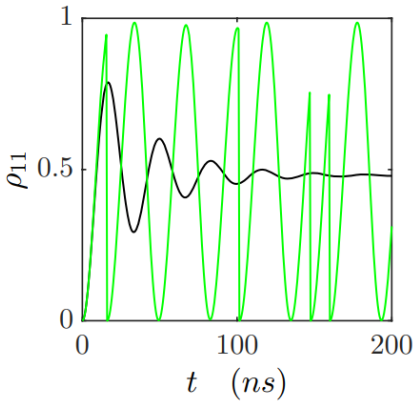

Figure 4.6: Simulação com MCWF para obtenção de trajetórias quânticas (linha verde) e para uma média de várias possíveis trajetórias do sistema (linha preta) [11].

4.5 Conclusão

Em síntese, a série de experimentos de fluorescência telegráfica sugerem que a interpretação probabilística para os saltos quânticos é a que mais se adequa aos resultados. Atrelado a isso, uma hipótese conciliadora entre as duas visões acerca da natureza das transições associa o comportamento discreto dos saltos com o efeito Zeno, como consequência do processo de medição do sistema em intervalos temporais muito pequenos e a consequente não evolução temporal do sistema. Por fim, foram demonstradas maneiras práticas de simular o fenômeno dos saltos quânticos computacionalmente, avaliando tanto os processos de absorção e emissão estimulada, quanto o processo de emissão espontânea, obtendo os limites esperados para sistemas em diferentes regimes e norteando caminho para simulações numéricas de processos com demanda experimental muito mais complexa.

Bibliografia

[1] BOHR, N. I. *On the constitution of atoms and molecules, The London, Edinburgh, and Dublin Philosophical Magazine and Journal of Science*. v. 26, n. 151, p. 1-25, 1913.

[2] SCHRÖDINGER, E. *Are there quantum jumps? Part II. The British Journal for the Philosophy of science*.v. 3, n. 11, p. 233-242, 1952.

[3] RICHARD J. COOK, *Quantum Jumps, E. Wolf, Progress In Optics Xxviii Elsevier Science Publishers B.v.*.1990.

[4] NAGOURNEY, W. SANDBERG, J. DEHMELT, H *Shelved optical electron amplifier: Observation of quantum jumps. Physical Review Letters*.v. 56, n. 26, p. 2797, 1986..

[5] NEUHAUSER, W., M. HOHENSTATT, P. TOSCH, and H. DEHMELT *Localized visible Ba mono-ion oscillator*.Phys. Rev. A 22,1137, 1980.

[6] BERGQUIST, J. C., R. G. HULET,W. M. ITANOand D. J. WINELAND *Observation of Quantum Jumps in a Single Atom*.Phys. Rev. Lett. 57, 1699.

[7] SAUTER,TH., R. BLATT,W. NEUHAUSER and P. E. TOSCHE *Observation of Quantum Jumps*.Phys. Rev. Lett. 57, 1696, 1986.

[8] COOK,R. J. *Telegraphic Atomic Fluorescence, in: Lasers, Molecules and Methods*.p. 715. 1989.

[9] ITANO,W. M., D. J. HEINZEN,J. J. BOLLINGER and D. J. WINELAND, *Quantum Zeno effect*.Phys. Rev. A 41, 2295.

[10] Chang Jae Lee *Quantum Jump Approach to Stimulated Absorption and Emission, Bull. Korean Chem. Soc.*.2006, Vol. 27, No. 8.

[11] COURTEILLE, Ph. W. *Quantum Mechanics applied to Atoms and Light, jun. de 2021. 1070 f. Notas de Aula. Universidade de São Paulo, Instituto de Física de São Carlos.*.

5

Observation of super- and subradiant spontaneous emission of two ions

Gustavo Henrique de França

Instituto de Física de São Carlos, Universidade de São Paulo, 13560-970 São Carlos, SP, Brazil

Abstract: This paper presents theoretical aspects of super- and subradiant spontaneous emission of two ions using the Dicke model, emphasizing the significance of collective interactions within the system. Experimental techniques are introduced, enabling the practical observation of these effects. These techniques involve selective excitation of specific states of the atoms, manipulation of dipole moments with phase differences, and control over the distance between the ions. The second-order correlation is investigated, revealing the intricate interplay between the ions and their collective behavior. Furthermore, the paper explores potential applications of super- and subradiance, including enhanced quantum information processing, quantum simulations and precision metrology. This work contributes to a deeper understanding and practical utilization of super- and subradiant spontaneous emission in the context of two-ion systems.

Keywords: Quantum Optics, Superradiance, Subrradiance, Two Ions, Collective Effects

5.1 Introduction

Quantum systems composed of multiple interacting particles often exhibit interesting collective behaviors that transcend the properties of individual constituents. The study of such phenomena has led to groundbreaking insights in various fields, ranging from condensed matter physics [1, 2, 3] to quantum information science [4, 5]. One intriguing collective quantum effect is the phenomenon of super- and subradiance, which arises from the cooperative emission of radiation by an ensemble of emitters [6].

In recent years, there has been a surge of interest in exploring super- and subradiant spontaneous emission in systems comprising two ions [7, 8, 9]. These experiments have shed new light on the intricate interplay between the internal degrees of freedom of quantum emitters and their interaction with the electromagnetic field. By manipulating the quantum states and coupling strengths of these ions, researchers have successfully observed and characterized the emergence of cooperative emission phenomena, opening up exciting avenues for both fundamental investigations and practical applications [10].

This paper will delve into the theoretical and experimental techniques employed to observe and manipulate super- and subradiant spontaneous emission in systems involving two ions. Furthermore, it will discuss the implications of these findings for applications such as quantum information processing, quantum simulations, and precision metrology. The understanding gained from these investigations holds great promise for future advancements in the realm of collective quantum phenomena and may pave the way for the realization of novel quantum technologies.

5.2 Super- and Subradiant Spontaneous Emission

A crucial factor in the study of the interaction between only two atoms is the distance between them. In several experiments involving a pair of trapped cold ions, interaction effects were not observed precisely due to the atom-atom distance. Dehmelt [11] experimentally produced a trap for two atoms with a distance of 3 μm and still did not observe interactions. Eichmann [12] studied Bragg scattering using two captured ions separated by $> 15\lambda$, with λ been the wavelength of the light, and once again, no inter-

action was observed. Therefore, the observation of collective spontaneous emission $\Gamma(R)$ for this minimum number of atoms is given as a function of the distance R between them. The super- and subradiance effects are defined by emission rates greater or smaller, respectively, than that generated by a single ion under the same conditions.

To mathematically model the system of interest, we employ Dicke's model, which allows the simplification of a system with many atoms by considering collective behavior and treating the atoms as an effective single entity [6]. In this model, the individual atoms are assumed to interact with each other and the electromagnetic field, leading to coherent effects on a macroscopic scale. By considering the collective properties of the system, such as the total angular momentum and the average atomic excitation, Dicke's model enables a reduction in complexity compared to analyzing each atom individually. In Dicke's theory, instead of treating the two-level atoms independently, we approach the system as a single four-level atom (Fig. 5.1). The higher level $|e\rangle$ corresponds to when both atoms are excited, while the lower level $g\rangle$ represents their ground states. Additionally, there are two collective states denoted as $|+\rangle$ and $|-\rangle$ that are superpositions of the states where only one of the atoms is in the excited state [6].

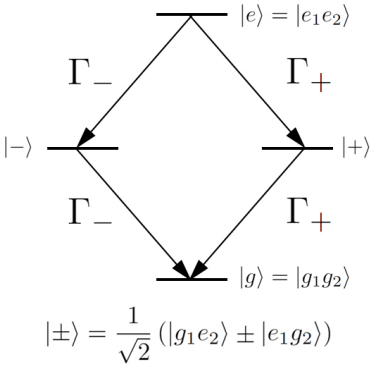

Figure 5.1: Diagram of the four-level system corresponding to the two two-level atoms coupled in the Dicke system. $\Gamma_\pm$ represents the spontaneous decay to and from the states $|\pm\rangle$, which are superpositions of states where only one ion is excited. The excited and ground states are represented by $|e\rangle = |e_1e_2\rangle$ and $|g\rangle = |g_1g_2\rangle$.

The master equation formalism can be used to derive the decay rate between energy levels in function of the distance R, which can be approximated to

$$\Gamma_\pm(R) = \Gamma_0\left(1 \pm \frac{3}{2}\frac{\sin kR}{kR} + ...\right) \tag{5.1}$$

where Γ_0 is the decay rate for a single ion and $k = 2\pi/\lambda$ [10]. What Eq. 5.1 represents is a superposition of electromagnetic waves emitted by atoms at different positions relative to the detector. We consider the system initially populated in its excited state and then calculate the decay rate between energy levels, with superradiance been equivalent to $\Gamma_+(R) > \Gamma_0$ and the subradiance $\Gamma_- < \Gamma_0$. Experimentally, this would be equivalent to considering an initial pulse that elevates the system to the state $|e\rangle$, and then measuring the rate at which the photons emitted by spontaneous emission are detected by a photodetector. The decay curve $W(R,t)$ produced by the photon statistics is given by the sum of the four transitions as

$$\begin{aligned} W(R,t) = \rho_e(t)\left[\Gamma_+(R) + \Gamma_-(R)\right] \\ +\rho_+(t)\Gamma_+(R) + \rho_-(t)\Gamma_-(R) \end{aligned} \tag{5.2}$$

where the terms $\rho_j(t)$ correspond to the diagonal elements of the density matrix $\rho(t)$ given by the master equation. In the region where $kR \leq 1$, which means that the wavelength of the field is close to the distance between the ions, it is relatively easier to determine when super- and subradiance occur. This can be visualized through the Eq. 5.1, where we observe that $|\Gamma_\pm - \Gamma_0| > 1$. However, as kR increases $|\Gamma_\pm - \Gamma_0| \approx 0$ and then super- and subradiance become increasingly indistinguishable, therefore, harder to be observed experimentally.

To observe a strong signal of super- and subradiant spontaneous emission from two ions, it is necessary to perform separate excitations of either $|+\rangle$ or $|-\rangle$, stimulating the population of one of these states. One way to select a state to populate is by inducing dipole moments with a phase difference on the atoms. DeVoe and Brewer [10] propose an experiment capable of coherently exciting the population of the states $|\pm\rangle$ using a laser pulse that forms an angle θ with the trap axis and has a wave vector $\vec{k}$ with a phase difference proportional to the distance between the atoms, denoted as $\Phi = \vec{k}\cdot\vec{R}$. The populations of the $|\pm\rangle$ states can then be expressed in terms of the single-atom density matrices as follows:

$$\rho_\pm = |\rho_{eg}|^2(1 \pm \cos\Phi) \tag{5.3}$$

Therefore, the excitations can be adjusted to occur for the $|+\rangle$ or $|-\rangle$ state by adjusting the distance R or the incidence of the laser angle θ, so that the phase difference is either $\Phi = 0$ or $\Phi = \pi$. They

were able to experimentally verify these theoretical results using Ba^{+}_{138}. The technical details of the apparatus are provided in the original paper [10]. In summary, they measured the $\Gamma(R)$ of the $P_{1/2}$ to $S_{1/2}$ transition in a crystal of two ions produced with a distance R of 1470 nm when the trap is driven at 500V, but which could vary from 1380 to 1540 nm with a variation of -10 to +5V. The ions formed an angle of 40 degrees with respect to the horizontal plane, so to produce a phase difference of $\Phi = \pi$, an incident beam at an angle $\theta = 16°$ was required for $R = 1470$ nm. Under these conditions, the state $|-\rangle$ was predominantly excited, and by varying the distance between the ions, we can observe the different states being stimulated and, consequently, the super- or subradiance occurring. Fig. 5.2 shows the variation in the spontaneous emission of the crystal as a function of the distance R between the ions, compared to the spontaneous emission of a single ion.

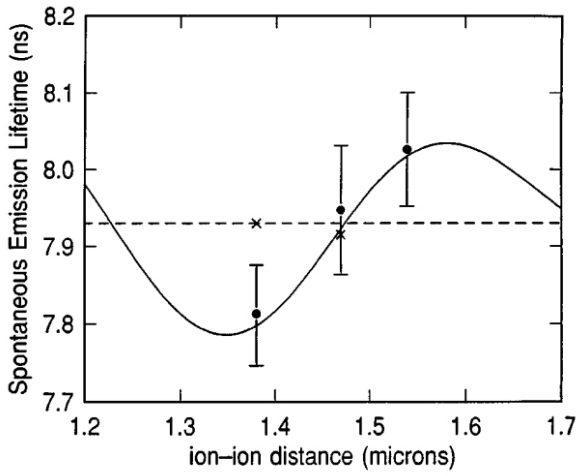

Figure 5.2: Experimental data points are shown for the lifetimes at 1380, 1470, and 1540 nm, in comparison to the measured lifetime for a single ion (dashed line) using the same apparatus [10].

Separate measurements of a single ion yielded an average lifetime $\tau = 1/\Gamma$ of 7.93 ± 0.03 ns, indicated by the dotted line in the figure. A superradiant point can be identified at 1380 nm, which is $1.5\% \pm 0.8\%$ below the value for a single ion. Additionally, a subradiant point is observed at 1540 nm, which is $1.2\% \pm 0.9\%$ above the single-ion value.

An equivalent experiment was conducted by Mlynek et al. [9] using two artificial atoms comprised of superconducting qubits in the "bad cavity" limit, where the cavity decay rate κ is much larger than the coupling strength and the atomic decay Γ_0. These qubits were coupled to a single coplanar waveguide resonator within a quantum circuit. Based on the results obtained from simulating the decay of individual atoms and the collective decay, they reach the conclusion that when both qubits are prepared in the state $|e\rangle$ and synchronized with the resonator, a distinct collective superradiance is observed. Furthermore, they can populate what they refer to as the bright state, equivalent to the state $|+\rangle$ depicted in Fig. 5.2. They observe that the decay from this state to the ground state is greater compared to the decay from the single states $|g_1 e_2\rangle$ or $|e_1 g_2\rangle$ to the ground state, which is a direct consequence of the phenomenon of superradiance occurring only when considering collective interactions [9]. Fig. 5.3 shows the time-dependent emitted power P for a specific initial state and the deviation ΔP from the average power of a single qubit. It becomes evident, as indicated by the orange region, that there exists a difference between collective and individual decay, arising from the predicted dynamics of the two ions.

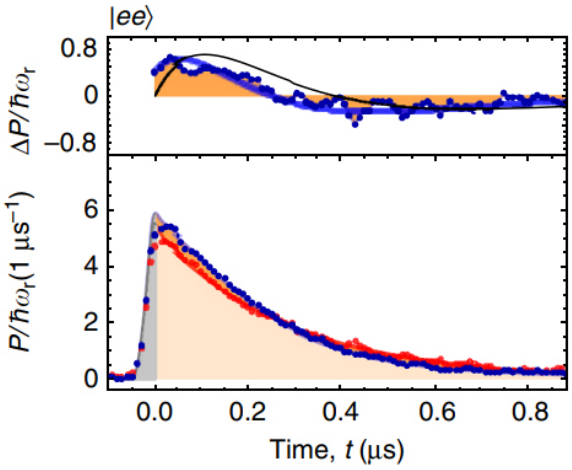

Figure 5.3: The time dependence of the emitted power P is shown for a specific initial state (bottom), along with the deviation ΔP (top) from the average power of a single qubit (red points). The collective decay for the initial state $|ee\rangle$ is examined. The experimental data (blue dots) are compared with a simple rate equation model (solid black lines) and full master equation simulations (solid blue lines). The orange area indicates the difference between the collective decay of the two qubits and the average decay of individual qubits, emphasizing the occurrence of super- and subradiance [9].

The analysis of the photon statistics of the transmitted light provides further insights into the phenomena of super- and subradiance. Richter et al. [13] proposed a pair of $^{40}Ca^{+}$ ions cooled by a laser on the $S_{1/2}$ - $P_{1/2}$ transition at 397 nm in free space. The scattered photons passed through a Hambury-Brown and Twiss interferometer, which consisted of a nonpolarizing 50/50 beam splitter and two camera detectors. The different lifetimes between the individual ion and the pair naturally lead to a change in the second-order correlation measured from the interferometer, and the observed result precisely reflects the statistical difference between photons scattered by superradiance and subradiance.

They analyze the collective aspects of light emission from a spatial and temporal perspective. Spatially, there is a phase difference of π between two consecutive photons detected through the decay $|e\rangle \rightarrow |+\rangle \rightarrow |g\rangle$, and a phase difference of 0.1π when the decay is $|e\rangle \rightarrow |-\rangle \rightarrow |g\rangle$. Temporally, we observe that the photon autocorrelation function $g^{(2)}(r_1, r_2, \tau = 0)$ displays antibunching for $\delta(r_1) = \delta(r_2) = 0.1\pi$, and bunching for $\delta(r_2) = \delta(r_2) = \pi$, where $\delta(r)$ represents the optical phase accumulated by a photon recorded at position r when scattered by atom 1 with respect to a photon scattered by atom 2 [13]. Fig. 5.4 illustrates the curve of $g^{(2)}$ for both cases.

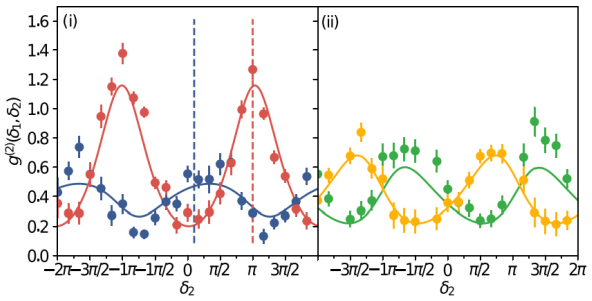

Figure 5.4: The curves represent cuts of histograms at $\tau = 0$, binned to $\delta(r_2)$. (i) Spatial superradiance is observed as indicated by the blue dots when $\delta(r_1) = 0.1\pi$ in the direction $\delta(r_2) \approx 0$. On the other hand, spatial subradiance is observed as indicated by the red dots when $\delta(r_1) = 1.05\pi$. (ii) Intermediate regimes between spatial superradiance and subradiance are observed for the second spontaneously scattered photon, when $\delta(r_1) = 0.7\pi$, this is represented by the yellow dots, and when $\delta(r_1) = 1.4\pi$, this is represented by the green dots [13].

They conclude that when a correlated pair of atoms emits light in free space, it exhibits remarkable collective behavior. This behavior includes spatial phenomena such as superradiance and subradiance, which are accompanied by photon antibunching and bunching, respectively.The properties of light emitted through fundamentally collective phenomena of ions have practical implications.

5.3 Technological applications

Super- and subradiant spontaneous emission in systems involving two ions have significant implications for various technological applications, including quantum information processing, quantum simulations, and precision metrology as follows.

Quantum Information Processing: Super- and subradiance can be utilized to enhance or suppress the emission of photons, which is essential for the implementation of quantum gates and the generation of entangled states. By controlling the collective emission properties, researchers can enhance the efficiency of photon generation in quantum networks and improve the fidelity of quantum operations. This can lead to advancements in quantum communication, quantum cryptography, and quantum computing [4, 5] .

Quantum Simulations: Systems involving two ions can serve as excellent platforms for simulating complex quantum systems and phenomena. Super- and subradiance enable the exploration of cooperative emission dynamics and the study of collective quantum effects. By engineering the ions' states and their interaction with the electromagnetic field, researchers can simulate a wide range of physical phenomena, including quantum phase transitions, quantum many-body systems, and quantum transport phenomena [14, 15].

Precision Metrology: Super- and subradiance offer opportunities for high-precision measurements and sensing applications. The collective emission properties can be exploited to enhance the detection sensitivity of certain physical quantities, such as electric or magnetic fields. By precisely controlling the collective emission properties, researchers can design systems that exhibit enhanced photon count statistics, reduced noise, and improved measurement precision. This has implications for precision metrology techniques, such as quantum metrology, quantum sensing, and quantum-enhanced imaging [16].

Fundamental Physics: Super- and subradiant spontaneous emission in systems involving two ions

offer opportunities to study fundamental aspects of light-matter interactions and quantum dynamics. These phenomena highlight the cooperative behavior of quantum emitters and their interactions with the quantized electromagnetic field. By exploring the interplay between collective effects, coherent control, and environmental factors, researchers can gain a deeper understanding of quantum mechanics, quantum electrodynamics, and the foundations of quantum physics [6, 9, 10].

In summary, super- and subradiant spontaneous emission in systems involving two ions have far-reaching implications for quantum information processing, quantum simulations, precision metrology, quantum control, and fundamental physics. These phenomena provide avenues for enhancing quantum operations, simulating complex systems, improving measurement precision, and advancing our understanding of quantum dynamics. Harnessing and controlling collective quantum effects in such systems opens up new opportunities for technological advancements and scientific discoveries.

5.4 Conclusion

In conclusion, the observation of super- and subradiant spontaneous emission of two ions represents a significant milestone in the study of collective quantum phenomena. Through careful experimental investigations and theoretical analyses, researchers have gained insights into the cooperative behavior of quantum emitters and their interaction with the electromagnetic field.

Theoretical models, such as the Dicke model, have provided a solid foundation for understanding the underlying principles governing super- and subradiance. These models have elucidated the role of collective states, quantum interference, and the interplay between emitters and the field in determining the emission properties of the system.

Experimental techniques have enabled the practical observation of the effects and the precise control and measurement of the emitted photons. These techniques have allowed researchers to observe and manipulate the super- and subradiant effects, providing experimental evidence that aligns well with theoretical predictions.

The implications of super- and subradiance extend beyond fundamental physics, with significant implications for quantum information processing, quantum simulations, and precision metrology. The ability to enhance or suppress the emission of photons in controlled ways opens up new avenues for quantum technologies, including improved quantum gates, efficient photon sources, and high-precision measurement devices.

Furthermore, the study of super- and subradiant spontaneous emission in systems involving two ions contributes to our understanding of fundamental quantum dynamics and the interplay between quantum emitters and the electromagnetic field. It sheds light on the cooperative behavior of quantum systems and the emergence of collective effects, providing valuable insights into the foundations of quantum mechanics.

As we continue to explore and refine our understanding of super- and subradiant spontaneous emission, there is immense potential for further advancements in both theoretical understanding and experimental applications. Future research could focus on exploring more complex systems, investigating novel control techniques, and expanding the range of applications, thereby unlocking the full potential of collective quantum phenomena.

Bibliografia

[1] Kankan Cong, Qi Zhang, Yongrui Wang, et al. *J Opt Soc Am B.* 33, 7, C80-C101 (2016).

[2] Trebbia, JB., Deplano, Q., Tamarat, P. et al. *Nat Commun.* 13, 2962 (2022).

[3] T. Laurent, Y. Todorov, A. Vasanelli, et al. *Phys Rev Lett.* 115, 187402 (2015).

[4] Zhen Wang, Hekang Li, Wei Feng, et al. *Phys Rev Lett.* 124, 013601 (2020).

[5] Scheibner, M., Schmidt, T., Worschech, L. et al. *Nat Phys.* 3, 106–110 (2007).

[6] R. H. Dicke *Phys Rev.* 93, 99 (1954).

[7] Eschner, J., Raab, C., Schmidt-Kaler *Nature.* 413, 495–498 (2001).

[8] S. Filipp, M. Göppl, J. M. Fink, et al. *Phys Rev A.* 83, 063827 (2011).

[9] J.A. Mlynek, A.A. Abdumalikov, C. Eichler1, A. Wallraff. *Nat Commun.* 5, 5186 (2014).

[10] R. G. DeVoe and R. G. Brewer *Phys Rev A.* 99, 043807 (1996).

[11] H. Dehmelt *Rev Mod Phys.* 62, 525 (1990).

[12] U. Eichmann, J. C. Bergquist, J. J. Bollinger, et al. *Phys Rev Lett.* 70, 2359 (1993).

[13] Stefan Richter, Sebastian Wolf, Joachim von Zanthier, Ferdinand Schmidt-Kaler *Phys Rev Research*. 5, 013163 (2023).

[14] Chen, X., Wu, Z., Jiang, M. et al. *Nat Commun*. 12, 6281 (2021).

[15] R. T. Sutherland *Phys Rev A*. 100, 061405 (2019)

[16] R. G. Brewer *Phys Rev Lett*. 77, 5153 (1996)

6

The Einstein-Podolski-Rosen hypothesis and its experimental falsification

Nathan Barbola Marucci

Instituto de Física de São Carlos, Universidade de São Paulo, 13560-970 São Carlos, SP, Brazil

Abstract: In a 1935 article entitled "Can quantum mechanical description of physical reality be considered complete?", Albert Einstein, Boris Podolsky, and Nathan Rosen argued that quantum mechanics was incomplete. The so-called EPR paradox was based on the principles of realism and locality. The completeness of quantum mechanics was debated for many years until John Bell proposed an inequality in 1964 to test hidden variable theories. However, the predictions of quantum mechanics, along with the experimental results that followed in the 1980s, strongly violated this inequality. Therefore, this work aims to point out the arguments used by those opposed to the completeness of quantum mechanics, as well as to present the development made by Bell to arrive at his inequality and describe an experiment conducted by physicist Alain Aspect.

6.1 Introduction

6.1.1 Determinism vs. Causality

As we know, in quantum mechanics, every observable is represented by a Hermitian operator whose eigenstates form a complete basis on which we can expand the quantum state of the system. Thus, let $\hat{A}$ be a Hermitian operator with discrete eigenvalues a'. We have:

$$\hat{A}\,|a'\rangle = a'\,|a'\rangle \quad \text{and} \quad |\Psi\rangle = \sum_{a'} c_{a'}\,|a'\rangle \tag{6.1}$$

Here, $|a'\rangle$ represents the eigenstates of $\hat{A}$ and satisfies the orthonormality condition:

$$\langle a''|a'\rangle = \delta_{a'a''} \tag{6.2}$$

Thus, the squared magnitude of the coefficients $c_{a'}$ gives the probability of obtaining the eigenvalue a' when measuring $\hat{A}$. Therefore, quantum mechanics exhibits a probabilistic nature.

On the other hand, once we know the initial quantum state of the system, we can determine how it evolves over time through the Schrödinger equation:

$$\hat{H}\,|\Psi\rangle = i\hbar\frac{\partial}{\partial t}\,|\Psi\rangle \tag{6.3}$$

Hence, in terms of the system's evolution, quantum mechanics is deterministic.

6.1.2 Realism

However, the aspect of quantum theory that tells us only the probability of obtaining a certain value when making a measurement troubled many physicists in the early 20th century, with Albert Einstein being the most emblematic among them. The so-called realists believed that nature should not be probabilistic, but completely deterministic, so that we should know the state of the system with precision. For them, quantum mechanics was not wrong, but incomplete; it lacked unknown variables, called **hidden variables**, which, together with the wave function $\Psi(x')$ given by

$$\Psi(x') = \langle x'|\Psi\rangle, \tag{6.4}$$

would fully characterize the physical system. Thus, since we wouldn't have prior knowledge of these hidden variables, we could only have access to probabilities.

On the other hand, the orthodox viewpoint believed that quantum mechanics was complete, that these hidden variables did not exist, and that nature was indeed probabilistic. However, this interpretation brings something difficult to conceive: **the**

collapse of the wave function. Due to the fact that successive measurements of the same quantity always result in the same value, it is necessary to impose that the wave function collapses. In other words,

$$|\Psi\rangle \xrightarrow{\hat{A} \text{ measurement}} |a'\rangle\,. \tag{6.5}$$

In addition to these two lines of thought at the time, there were the agnostics who refrained from seeking an answer to these questions, claiming that they were merely philosophical issues. What mattered to them was that quantum theory agreed with experimental observations.

6.2 EPR Paradox

6.2.1 Overview

In a 1935 article [1] titled "Can the quantum-mechanical description of physical reality be considered complete?", an thought experiment known as the EPR Paradox was proposed by Albert Einstein, Boris Podolsky, and Nathan Rosen. In the article, the three authors argued from a realist perspective that the description provided by quantum mechanics is incomplete. And for this, they utilized the phenomenon of **quantum entanglement**.

We will now summarize the argument used by them.

Consider two systems, I and II, that are allowed to interact from time $t = 0$ to $t = T$, after which it is assumed that there is no further interaction between the two parties. Let's denote the total wave function as Ψ. We cannot calculate the state in which each system remains after the interaction. This can only be done, according to quantum mechanics, through measurements that result in the collapse of the wave function.

Let $a_1,\ a_2,\ a_3,\ \cdots$ be the eigenvalues of some physical quantity $\hat{A}$, and $u_1(x_1),\ u_2(x_1),\ u_3(x_1),\ \cdots$ their respective eigenfunctions, where x_1 is the variable used to describe the first system. Then, the wave function Ψ can be expressed as:

$$\Psi(x_1, x_2) = \sum_n \psi_n(x_2) u_n(x_1) \tag{6.6}$$

where x_2 is the variable used to describe the second system. Here, $\psi_n(x_2)$ are the coefficients of the expansion of Ψ in a series of orthogonal functions $u_n(x_1)$.

Suppose that the quantity $\hat{A}$ of the first system is measured and the value found is a_k. Then, we can conclude that after the measurement of the first system, it is left in the state described by the wave function $u_k(x_1)$, and the second system in the state corresponding to $\psi_k(x_2)$. Thus, the wave packet described by Equation 6.6 is reduced to a single term $\psi_k(x_2)u_k(x_1)$.

However, the set of eigenfunctions $u_n(x_1)$ is determined by the choice of the observable $\hat{A}$. If instead we chose another observable, say $\hat{B}$, with eigenvalues $b_1,\ b_2,\ b_3,\ \cdots$, and with the respective eigenfunctions $v_1(x_1),\ v_2(x_1),\ v_3(x_1),\ \cdots$, then instead of Equation 6.6, we would have the following expansion:

$$\Psi(x_1, x_2) = \sum_s \varphi_s(x_2) v_s(x_1) \tag{6.7}$$

where $\varphi_s(x_2)$ are the new expansion coefficients. If the quantity $\hat{B}$ of the first system is measured and the value b_r is found, then the first system will be in the state with the corresponding wave function $v_r(x_1)$, and the second system will have the wave function $\varphi_r(x_2)$.

In this way, we can see that as a consequence of the different measurements performed on the first system, the second system can be left in states with two different wave functions. And since at the time of measurement the two systems no longer interact, no actual change can occur in the second system as a result of any measurement made on the first. Thus, it is possible to associate two different wave functions (ψ_k and φ_r) with the same reality (the second system after the interaction).

It turns out that the observables $\hat{A}$ and $\hat{B}$ can be chosen in such a way that they do not commute with each other, that is,

$$[\hat{A}, \hat{B}] \neq 0. \tag{6.8}$$

Thus, there is an uncertainty relationship between them given by the **Generalized Heisenberg Uncertainty Principle**:

$$\sqrt{\left\langle (\Delta\hat{A})^2 \right\rangle} \cdot \sqrt{\left\langle (\Delta\hat{B})^2 \right\rangle} \geq \frac{1}{2} |\langle [\hat{A}, \hat{B}] \rangle|. \tag{6.9}$$

This occurs, for example, in the case of the position $\hat{x}$ and the momentum $\hat{p}$ of a particle, where it is not possible to simultaneously know these two physical quantities with precision. From an orthodox point of view, this means that they do not possess simultaneous reality.

Therefore, we must prove that (1) the description of quantum mechanics is incomplete or (2) two non-commuting observables cannot have simultaneous physical reality. To do this, let us consider that

the description of nature by the wave function is complete. From the previous discussion about systems I and II, we are led to the conclusion that two physical quantities with non-commuting operators can have simultaneous reality. Thus, the negation of (1) implies the negation of (2), and we are forced to conclude that the description provided by quantum mechanics is incomplete.

David Bohm, in a 1957 paper [2], presented a simplified version of the EPR Paradox that turned the thought experiment into something closer to a feasible experiment. We will discuss this version next.

6.2.2 Spin Correlation

Consider a total spin 0 system consisting of two particles, A and B, each with spin 1/2. Thus, the system will be in the singlet spin state, given by:

$$|j=0, m=0\rangle = \frac{1}{\sqrt{2}}\left(|+-\rangle - |-+\rangle\right), \qquad (6.10)$$

where $|+-\rangle$ means that the first particle (A) has spin up and the second one (B) has spin down. The same argument holds for the state $|-+\rangle$.

Then, the two particles are separated by a process that does not influence the total spin of the system. After these particles are separated by a sufficiently large distance to stop interacting with each other, any component of the spin of the first particle (A) is measured, for example, using a Stern-Gerlach apparatus (Figure 6.1). Due to the fact that the total spin is still zero, we can conclude that the corresponding component of the spin of the other particle (B) is opposite to that of A.

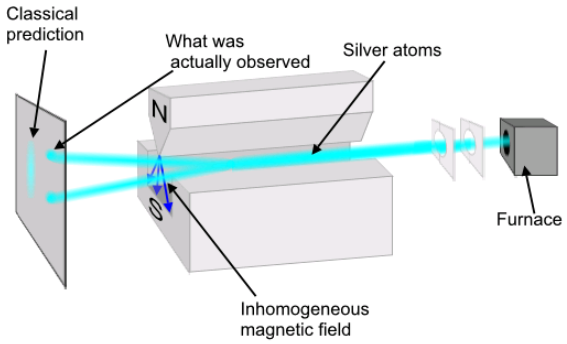

Figure 6.1: Scheme of the Stern-Gerlach Experiment

If it were a classical system, there would be no difficulty in interpreting the results above, since all spin components of each particle would be well-defined at each instant of time. Thus, each spin component of particle A would have a value opposite to that same component of B from the beginning. In other words, the two spin vectors would be completely correlated.

However, in quantum mechanics, a difficulty arises due to the fact that:

$$[S_i, S_j] = i\epsilon_{ijk}\hbar S_k, \qquad (6.11)$$

and only one spin component has a defined value at a time. Therefore, if the z-component is known, the x and y components become indeterminate and can be considered as a kind of random fluctuation. In fact, since

$$|S_z, \pm\rangle = \frac{1}{\sqrt{2}}\left(|S_x, +\rangle \pm |S_x, -\rangle\right), \qquad (6.12)$$

after measuring $\hat{S}_z$, there is a 50% chance of obtaining spin up or spin down when measuring $\hat{S}_x$.

Thus, the result for a component of B seems to depend on the type of measurement being performed on A. We can measure any spin component of particle A we want by simply rotating the experimental setup. According to quantum mechanics, it doesn't matter which component of particle A is measured, the corresponding component of particle B will have a defined value opposite to it. However, the question arises: How does particle B know which spin component of particle A is being measured, if they are separated by a large distance and there is no interaction between them or between particle B and the experimental setup?

Einstein referred to this phenomenon, in which the measurement of a property of one particle causes the wave function of another particle to instantaneously collapse, as "spooky action at a distance." And the main assumption of those who argued that quantum mechanics was incomplete was that no influence could propagate faster than the speed of light! This principle is called **locality**.

This problem would be easily solved from the realist perspective, as according to them, the spin of the two particles was already predetermined from the moment the system decayed.

The debate about whether nature was probabilistic or deterministic remained within the philosophical realm until a 1964 paper [3] titled "On the Einstein-Podolsky-Rosen paradox," where the physicist John Bell proposed an inequality that could be experimentally tested, putting the existence or non-existence of hidden variables to the test.

6.3 Bell's Theorem

To illustrate what was mentioned in subsection 6.2.2, let's consider the decay of a neutral pion in the initial singlet state into an electron and a positron.

$$\pi^0 \to e^- + e^+. \tag{6.13}$$

As we know, the electron and the positron have a spin of 1/2, so their components will have eigenvalues $\pm\hbar/2$. For simplicity, we will adopt $\hbar/2$ as the unit.

What Bell proposed was to calculate the average value of the spin product for a set of detector orientations. Let this average be denoted by $P(\mathbf{a}, \mathbf{b})$, where $\mathbf{a}$ is the unit vector giving the orientation of the spin component measurement for the first particle (let's say, the electron) and $\mathbf{b}$ is the unit vector giving the orientation of the spin measurement for the second particle (positron).

So, if the detectors are parallel ($\mathbf{b} = \mathbf{a}$), when we measure the electron's spin and obtain $+1$, we know that the positron's spin will be -1 and vice versa. The product between them will always be -1, and consequently, their average will also be:

$$P(\mathbf{a}, \mathbf{a}) = -1 \tag{6.14}$$

Similarly, if the axes are antiparallel ($\mathbf{b} = -\mathbf{a}$), then each product will result in $+1$, so

$$P(\mathbf{a}, -\mathbf{a}) = +1 \tag{6.15}$$

For arbitrary orientations, quantum mechanics predicts

$$\boxed{P(\mathbf{a}, \mathbf{b}) = -\mathbf{a} \cdot \mathbf{b}} \tag{6.16}$$

However, Bell discovered that this is incompatible with any theory of hidden variables!

Suppose that the "complete" state of the system is characterized by the hidden variable λ, which varies in a way that we neither control nor understand during the pion decay. Furthermore, assume that the electron's measurement result is independent of the orientation ($\mathbf{b}$) of the positron's detector. Then, there must exist a function $A(\mathbf{a}, \lambda)$ that gives the electron's measurement result, and another function $B(\mathbf{b}, \lambda)$ for the positron's measurement result. These functions can only take the values ± 1.

$$A(\mathbf{a}, \lambda) = \pm 1; \quad B(\mathbf{b}, \lambda) = \pm 1 \tag{6.17}$$

When the detectors are aligned, the results are perfectly correlated:

$$A(\mathbf{a}, \lambda) = -B(\mathbf{a}, \lambda) \tag{6.18}$$

and this is true for all λ.

Obviously, the average of the product of the measurements will be

$$P(\mathbf{a}, \mathbf{b}) = \int \rho(\lambda) A(\mathbf{a}, \lambda) B(\mathbf{b}, \lambda) \mathrm{d}\lambda \tag{6.19}$$

where $\rho(\lambda)$ is a probability density for the hidden variable. And, like any probability density, it must be non-negative and satisfy the normalization condition:

$$\int \rho(\lambda) \mathrm{d}\lambda = 1 \tag{6.20}$$

Using Equation 6.18, we can eliminate B in Equation 6.19

$$P(\mathbf{a}, \mathbf{b}) = -\int \rho(\lambda) A(\mathbf{a}, \lambda) A(\mathbf{b}, \lambda) \mathrm{d}\lambda \tag{6.21}$$

And, if $\mathbf{c}$ is another unit vector, then

$$P(\mathbf{a}, \mathbf{b}) - P(\mathbf{a}, \mathbf{c}) = -\int \rho(\lambda) \left[A(\mathbf{a}, \lambda) A(\mathbf{b}, \lambda) - A(\mathbf{a}, \lambda) A(\mathbf{c}, \lambda) \right] \mathrm{d}\lambda \tag{6.22}$$

Since $[A(\mathbf{b}, \lambda)]^2 = 1$, we have:

$$P(\mathbf{a}, \mathbf{b}) - P(\mathbf{a}, \mathbf{c}) = -\int \rho(\lambda) \left[1 - A(\mathbf{b}, \lambda) A(\mathbf{c}, \lambda) \right] A(\mathbf{a}, \lambda) A(\mathbf{b}, \lambda) \mathrm{d}\lambda \tag{6.23}$$

But it follows that $-1 \leq [A(\mathbf{a}, \lambda) A(\mathbf{b}, \lambda)] \leq +1$. Moreover, $\rho(\lambda) \left[1 - A(\mathbf{b}, \lambda) A(\mathbf{c}, \lambda) \right] \geq 0$. Therefore, we can conclude that

$$\begin{aligned} &|P(\mathbf{a}, \mathbf{b}) - P(\mathbf{a}, \mathbf{c})| \\ &\leq \int \rho(\lambda) \left[1 - A(\mathbf{b}, \lambda) A(\mathbf{c}, \lambda) \right] \mathrm{d}\lambda \end{aligned} \tag{6.24}$$

Or, more simply,

$$\boxed{|P(\mathbf{a}, \mathbf{b}) - P(\mathbf{a}, \mathbf{c})| \leq 1 + P(\mathbf{b}, \mathbf{c})} \tag{6.25}$$

Equation 6.25 is the famous **Bell's Inequality**, and it can be experimentally tested in **Bell tests**. If it is satisfied, nature respects the principle of locality, and hidden variables exist. If the inequality is not satisfied, nature is non-local, and hidden variables do not exist.

It is easy to see that the prediction of quantum mechanics (Equation 6.16) is incompatible with Bell's inequality. In fact, consider Figure 6.2. According to the prediction of quantum mechanics, we should have

$$P(\mathbf{a}, \mathbf{b}) = 0 \quad \text{and} \quad P(\mathbf{a}, \mathbf{c}) = P(\mathbf{b}, \mathbf{c}) = -0.707 \tag{6.26}$$

However,

$$0.707 \nleq 1 - 0.707 = 0.293 \qquad (6.27)$$

This violates Bell's inequality, demonstrating the non-locality of quantum mechanics.

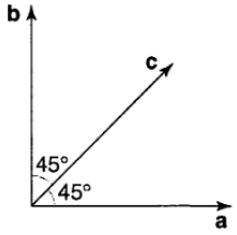

Figure 6.2: Orientation of the detectors

6.4 Aspect's Experiment

In 1969, Bell's Theorem was extended by Clauser, Horne, Shimony, and Holt (CHSH inequality) to include actual systems [4], providing an experimental test for all local hidden-variable theories.

During the years 1980 to 1982, the French physicist Alain Aspect conducted a series of experiments with entangled photons in order to test Bell's inequality. Below, we describe one of these experiments [5].

This experiment employed the $4p^2\ ^1S_0 - 4s4p\ ^1P_1 - 4s^2\ ^1S_0$ cascade in calcium (Figure 6.3). This cascade yields two visible photons, ν_1 (551.3 nm) and ν_2 (422.7 nm), correlated in polarization. Calcium atoms are selectively excited to the upper level of the cascade from the ground state through two-photon absorption. Calcium is irradiated by two laser beams. The first laser beam ($\lambda_K = 406.7$ nm) is provided by a single-mode krypton ion laser, and the second laser is a single-mode Rhodamine dye laser tuned to resonance for the two-photon process ($\lambda_D = 561$ nm).

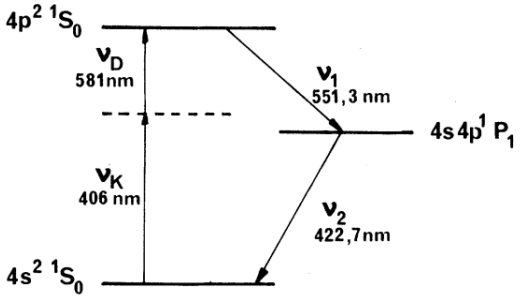

Figure 6.3: Relevant levels of calcium.

Fluorescence is then collected. Figure 6.4 shows a schematic diagram of the apparatus used. All the optical elements are antireflection coated. Polarizers I and II are inclined at nearly the Brewster's angle (zero reflectance). The transmittance ϵ_M^i and ϵ_m^i of the polarizers (i = 1 or 2) for parallel or perpendicular polarized light were then measured: $\epsilon_M^1 = 0.971 \pm 0.005$, $\epsilon_m^1 = 0.029 \pm 0.005$, $\epsilon_M^2 = 0.968 \pm 0.005$, and $\epsilon_m^2 = 0.028 \pm 0.005$.

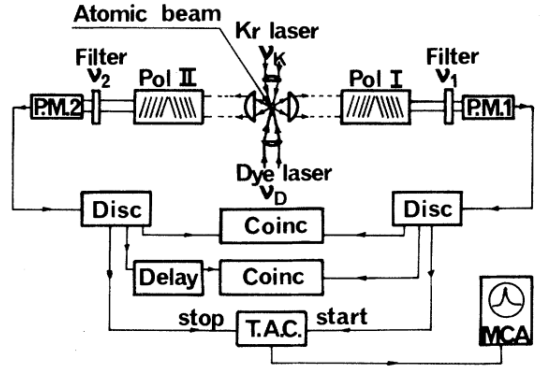

Figure 6.4: Schematic diagram of the apparatus and electronics.

The correlation rate $R(\mathbf{a}, \mathbf{b})$ between polarizer I in the direction $\mathbf{a}$ and polarizer II in the direction $\mathbf{b}$, the correlation rate $R_1(\mathbf{a}')$ with polarizer II removed and polarizer I in the direction $\mathbf{a}'$, the correlation rate $R_2(\mathbf{b}')$ with polarizer I removed and polarizer II in the direction $\mathbf{b}'$, and the correlation rate R_0 with both polarizers removed were then measured. Quantum mechanics predicts that:

$$R(\varphi)/R_0 = \frac{1}{4}(\epsilon_M^1 + \epsilon_m^1)(\epsilon_M^2 + \epsilon_m^2) + \frac{1}{4}(\epsilon_M^1 - \epsilon_m^1)(\epsilon_M^2 - \epsilon_m^2)F\cos(2\varphi) \qquad (6.28)$$

and

$$R_i/R_0 = \frac{1}{2}(\epsilon_M^i + \epsilon_m^i), \quad \text{for} \quad i = 1 \quad \text{or} \quad 2 \qquad (6.29)$$

where $\varphi = (\mathbf{a}, \mathbf{b})$ is the angle between these two orientations and $F = 0.984$ is an equipment adjustment parameter.

Figure 6.5 presents the normalized graph of $R(\varphi)/R_0$ as a function of the angle φ. The points represent the experimental data, and the solid curve is the result predicted by quantum mechanics (Equation 6.28 and Equation 6.29).

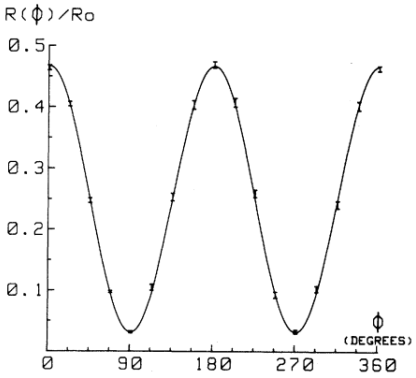

Figure 6.5: Normalized coincidence rate as a function of the relative polarizer orientation.

The generalized Bell theorem yields the following inequality:

$$-1 \leq S \leq 0 \tag{6.30}$$

where $S = [R(\mathbf{a}, \mathbf{b}) - R(\mathbf{a}, \mathbf{b}') + R(\mathbf{a}', \mathbf{b}) + R(\mathbf{a}', \mathbf{b}') - R_1(\mathbf{a}') - R_2(\mathbf{b}')]/R_0$.

We can see that the maximum violation of the inequality (Equation 6.30) is predicted by Equation 6.28 and Equation 6.29 for the set of orientations shown in Figure 6.6.

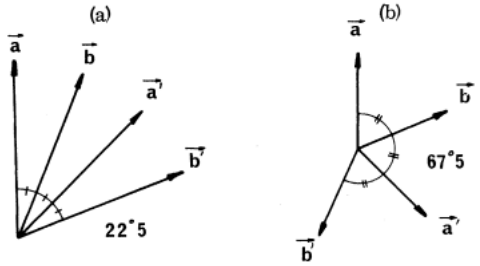

Figure 6.6: Orientations leading to the maximum violations of generalized Bell inequalities.

Thus, the experimental value obtained for S in the configuration displayed in Figure 6.6 was $S_{exp} = (0.126 \pm 0.014)$. This result violates Equation 6.30 and is consistent with the result predicted by quantum mechanics $S_{QM} = 0.118 \pm 0.005$.

6.5 Conclusion

Quantum mechanics is one of the most successful theories, and through the works utilizing entangled photons by Alain Aspect, John Clauser, and Anton Zeilinger, its completeness and non-locality have been demonstrated. It is no wonder that these three physicists were awarded the Nobel Prize in Physics in 2022 for these contributions, paving the way for the development of quantum computers, quantum networks, and quantum encrypted communication.

Bibliografia

[1] A. Einstein, B. Podolsky, and N. Rosen. Can quantum-mechanical description of physical reality be considered complete? *Phys. Rev.*, 47:777–780, May 1935.

[2] D. Bohm and Y. Aharonov. Discussion of experimental proof for the paradox of einstein, rosen, and podolsky. *Phys. Rev.*, 108:1070–1076, Nov 1957.

[3] J. S. Bell. On the einstein podolsky rosen paradox. *Physics Physique Fizika*, 1:195–200, Nov 1964.

[4] John F. Clauser, Michael A. Horne, Abner Shimony, and Richard A. Holt. Proposed experiment to test local hidden-variable theories. *Phys. Rev. Lett.*, 23:880–884, Oct 1969.

[5] Alain Aspect, Philippe Grangier, and Gérard Roger. Experimental tests of realistic local theories via bell's theorem. *Physical Review Letters*, 47:460–463, 1981.

[6] David Bohm. A suggested interpretation of the quantum theory in terms of "hidden" variables. i. *Phys. Rev.*, 85:166–179, Jan 1952.

[7] J. J. Sakurai and Jim Napolitano. *Modern Quantum Mechanics*. Cambridge University Press, 3 edition, 2020.

[8] David J. Griffiths and Darrell F. Schroeter. *Introduction to Quantum Mechanics*. Cambridge University Press, 3 edition, 2018.

7

Bose-Einstein condensation

Otávio Perez Palamoni

Instituto de Física de São Carlos, Universidade de São Paulo, 13560-970 São Carlos, SP, Brazil

Abstract: This article provides an overview of the differences between Fermions and Bosons, focusing on Bose-Einstein condensates (BECs). Some examples are explored such as trapping an ideial boson gas in a three-dimensional harmonic potential, which enhances the condensation rate when compared with a box. The article also deduce the Gross-Pitaevskii Equation, which distinguishes between ideal and real gases in the context of BECs. Visualizations of BECs from past and present are presented, showcasing the progress in studying these quantum phenomena. Overall, this article offers valuable insights into quantum physics and the potential practical implications of BECs in various scientific fields.

7.1 Introduction

The Bose-Einstein Condensate (BEC) was initially conceptualized by Albert Einstein in 1925, building upon the earlier work of Satyendra Nath Bose, published the previous year. Bose-Einstein condensation involves the cooling of a high-density gas of bosons, particles that do not interact with each other, below the critical temperature (TC) - also known as the condensate temperature - resulting in a macroscopic fraction of particles occupying the lowest energy state.

Due to the ability to achieve a substantial number of particles in a single quantum state, BECs serve as a remarkable tool for investigating statistical mechanics, quantum mechanics, condensed matter, and other related fields. The following are some noteworthy applications: Fundamental physics, atom interferometry, quantum optics, and photonics.

7.1.1 Fermions vs Bosons

Particles constitute the fundamental building blocks of matter and can be categorized into two primary classifications: **Fermions and Bosons**.

- **Fermions:** Fermions are particles that obey the Pauli exclusion principle, which states that no two identical fermions can occupy the same quantum state simultaneously, so they have half-integer spin values $(\frac{1}{2}, \frac{3}{2}, ...)$, they also adhere to the **Fermi-Dirac Distribution**.

$$f^r(E) = \frac{1}{e^{\frac{E-\mu}{k_B T}} + 1} \tag{7.1}$$

  Where $f^r(E)$ represents the occupation probability of the energy E and state r, E is the energy of the state, μ is the chemical potential, k_B is the Boltzmann constant, and T is the temperature of the system.

  Examples of Fermions: Electrons, Protons, and Neutrons.

- **Bosons:** Bosons are particles that do not obey the Pauli exclusion principle, allowing multiple identical bosons to occupy the same quantum state simultaneously. They have integer spin values $(1, 2, 3, ...)$, and they also follow the **Bose-Einstein Distribution**.

$$f^r(E) = \frac{1}{e^{\frac{E-\mu}{k_B T}} - 1} \tag{7.2}$$

Examples of Fermions: Photons, Gluons, and the W and Z bosons.

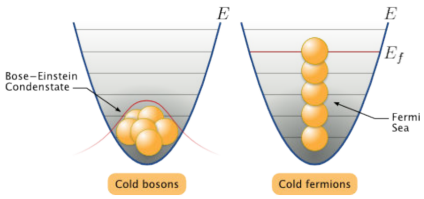

Figure 7.1: Visual representation of the difference between Fermions and Bosons.

7.1.2 The ideal Bose gas with an 3D harmonic potential

At high temperatures, a gas can be conceptualized as a collection of numerous billiard balls possessing a velocity denoted as v. The numeric density of the gas is inversely proportional to the cube of the mean distance between colliding particles (d), meaning that as d decreases, the density increases. However, as the temperature decreases, a different phenomenon comes into play: the wave-like behavior of particles becomes significant.

A significant portion of the particles contributes to the formation of the large matter-wave. However, it is worth noting that not all particles participate in this wave. In the hypothetical situation of reaching absolute zero temperature (0 K), all particles would occupy the ground state, leading to the creation of a pure Bose-Einstein Condensate (BEC) within an enormous matter-wave. Unfortunately, reaching absolute zero is unattainable due to the law of thermodynamics. The ability to approach such low temperatures allows researchers to observe and analyze the behavior of matter on a quantum scale, contributing to our understanding of the fundamental principles of physics.

Supposing a trapped gas be subjected to an external potential. In Statistical Physics, we have the following large partition function Ξ for non-interacting bosons gas:

$$\Xi(\beta,\varepsilon,\mu) = \prod_{r\in} \frac{1}{1-e^{-\beta\varepsilon_r-\mu}}, \beta \equiv \frac{1}{k_B T} \tag{7.3}$$

Equation 7.3 can be rewrite as:

$$ln\left[\Xi(\beta,\varepsilon,\mu)\right] = -\sum_{r\in\{states\}} ln\left(1-\zeta e^{-\beta\varepsilon_r}\right) \tag{7.4}$$

In equation 7.4 we have that $\zeta = e^{\beta\mu}$ is the system fugacity. The total number of particles N can be obtained using equation 7.4.

$$N = \zeta\frac{d}{d\zeta}(\Xi) = \sum_{r\in\{states\}} \frac{1}{\zeta^{-1}e^{\beta\varepsilon_r}-1}$$
$$\Rightarrow f^r = \frac{1}{\zeta^{-1}e^{\beta\varepsilon_r}-1} \tag{7.5}$$

In the quantum realm, bosons exhibit a nonpositive chemical potential ($\mu \leq 0$). As the temperature decreases, the chemical potential increases until it reaches zero at the critical temperature. Below the critical temperature, the chemical potential remains at zero. This unique behavior is indicative of Bose-Einstein Condensation and underlines its significance.In this scenario, the fugacity $\zeta = 1$, and the energy of the ground state is much smaller than the product of Boltzmann's constant and the temperature $\varepsilon \ll kT$ These conditions result in the occupation of the ground state becoming macroscopic. This macroscopic occupation is a defining characteristic of Bose-Einstein Condensation. It stems from a large number of particles in a single state, leading to the formation of a coherent matter wave through the superposition of multiple De Broglie waves from each particle in the system.

It is important to note that as the fugacity decreases (corresponding to higher temperatures), the occupation of the ground state diminishes, pushing the particles towards excited states. This transition corresponds to the classical regime, where the number of particles in each state is microscopic. In this regime, the quantum behavior becomes imperceptible. The classical regime arises from low fugacity values due to high temperatures, rendering quantum statistics unobservable. Mathematically, in the limit of low temperature, the expression for f^r in equation 7.4 tends towards ∞. This means that there is a macroscopic number of particles in the ground state.

$$f^0 = \lim_{r\to 0}(f^r) \to \infty \tag{7.6}$$

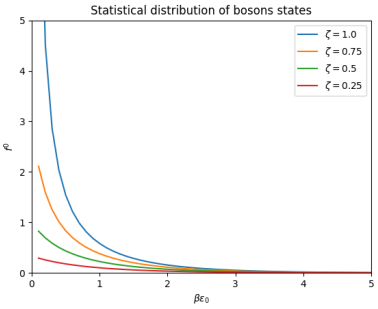

Figure 7.2: Statistical distribution of bosons states for three different values of fugacity (ζ) for the ground state ($r = 0$). All values converge to 0 as $x \to \infty$.

The Critical temperature (T_c) denotes the temperature at which a phase transition takes place. For a uniform gas confined in a trap, this critical temperature can be determined using the following relation:

$$T_c = C.\frac{\hbar^2 n^{\frac{2}{3}}}{mk_B} \tag{7.7}$$

Where C is a constant that depends on the trap, $\hbar \ll 1.055\times10^{-34} Js$ is the reduced Planck constant, n is the numerical density of particles and m is the mass of each particle. To determine the constant value, we use the quantum states degeneracy ρ. We will consider a gas trapped in a potential V that is a 3D harmonic oscillation, then the potential V can be expressed as follows:

$$V(x,y,z) = \sum_{i=1}^{3} \frac{m}{2} w_i^2 i^2 = \frac{m}{2}\left(w_x^2 x^2 + w_y^2 y^2 + w_z^2 z^2\right) \tag{7.8}$$

To solve this problem, first, we use equation 7.9, which is the time-independent Schrödinger equation.

$$\hat{H}\left|\psi\right\rangle = E\left|\psi\right\rangle, \hat{H} = -\frac{\hbar^2}{2m}\nabla^2 + \vec{V} \tag{7.9}$$

This leads to the following equations for each axis:

$$\left(\frac{\partial^2}{\partial i^2} - \frac{m^2 w_i^2}{\hbar^2 i^2}\right)\left|\psi\right\rangle = \frac{-2mE}{\hbar^2}\left|\psi\right\rangle \tag{7.10}$$

Assuming that $\alpha = \sqrt{\frac{mw_i}{\hbar}} i$ and $\beta = \frac{2mE}{\hbar^2 w_i}$, equation 7.10 turns into equation 7.11.

$$\frac{d^2}{d\alpha^2}\psi(\alpha) - \alpha^2\psi(\alpha) = \beta\psi(\alpha) \tag{7.11}$$

Equation 7.11 is known as the Hermite differential equation and its solutions are given by the Hermite polynomials, so the eigenvalues for the system can be expressed as shown in equation 7.12

$$E = \left(n_x + \frac{1}{2}\right)\hbar w_x + \left(n_y + \frac{1}{2}\right)\hbar w_y + \left(n_z + \frac{1}{2}\right)\hbar w_z \tag{7.12}$$

Assuming an $G(\varepsilon)$ the number of particules with energy at $\varepsilon = \varepsilon_x + \varepsilon_y + \varepsilon_z$, and considering that $\hbar w_i \ll \varepsilon$. The following expression can be determined using equation 7.12.

$$G_\varepsilon = \frac{1}{(\hbar w_x)(\hbar w_y)(\hbar w_z)} \int_0^\varepsilon d\varepsilon \int_0^{\varepsilon-\varepsilon_x} d\varepsilon_y \int_0^{\varepsilon-\varepsilon_x-\varepsilon_y} d\varepsilon_z \tag{7.13}$$

$$G_\varepsilon = \frac{\varepsilon^3}{6\hbar^3 w_x w_y w_z} \tag{7.14}$$

Since the degeneracy ρ is the number of particles with energy between ε and $\varepsilon + d\varepsilon$, ρ can be found using equation 7.14.

$$\rho(\varepsilon) = \frac{d}{d\varepsilon}G(\varepsilon) = \frac{1}{2\hbar^3 w_x w_y w_z}\varepsilon^2 = C_3\varepsilon^2 \tag{7.15}$$

By defining this phase transition as when the excited states are saturated, forcing any new particle go to the ground state. In this situation, the chemical potential is minimum ($\mu = 0$). We can describe this situation mathematically assuming the thermodynamics limit and transforming the number series in integral:

$$N = N_0 + \int_0^\infty f^r \rho(\varepsilon) d\varepsilon \Rightarrow \begin{cases} 0, T > T_c \\ 1 - \frac{1}{N}\int_0^\infty n_\varepsilon \rho(\varepsilon) T \leq T_c \end{cases} \tag{7.16}$$

N_0/N is the **condensed fraction** and it shows the system particules fractions that are in ground state and n_ε is the occupancy of states with energy ε. For the condensate fractions, we find that:

$$\frac{N_0}{N} = 1 - \frac{1}{N}\int_0^\infty \left(\frac{1}{e^{\beta\varepsilon} - 1}\right)(C_3\varepsilon^2)d\varepsilon = 1 - \frac{C_3}{N}\int_)^\infty \frac{\varepsilon^2}{e^{\beta\varepsilon}}d\varepsilon$$
$$= 1 - \frac{C_3}{N\beta}\Gamma(3)\zeta(3) \tag{7.17}$$

So $\Gamma(n) = (n-1)!$ for $n \in \mathbb{N}$ and $\zeta(n) = \sum_{k=1}^{\infty}\frac{1}{k^n}$ the zeta function. When $T = T_c$, then $N_0 = 0$, in this case equation 7.17 leads to the following expression for the T_c:

$$0 = 1 - \frac{C_3}{N}\left(k_B T_c\right)^3 \Gamma(3)\zeta(3)$$
$$\Rightarrow T_c = \frac{\hbar}{k_B}\sqrt[3]{\frac{2N w_x w_y w_z}{\Gamma(3)\zeta(3)}} \approx 7.19\times10^{-12}\sqrt[3]{N w_x w_y w_z} \tag{7.18}$$

If we substitute a typical number of particles and frequencies found in the laboratory, we get the condensation temperature of hundreds of nanokelvin. Since we have the condensation temperature expression, we can simplify the condensate fraction expression and write it as a function of T_c:

$$\frac{N_0}{N} = 1 - \left(\frac{T}{T_c}\right)^3 \tag{7.19}$$

For a box, the same equation is described as

$$\frac{N_0}{N} = 1 - \left(\frac{T}{T_c}\right)^{\frac{3}{2}} \tag{7.20}$$

While both expressions represent the same fenomenum, equation 7.19 implies that atoms populate the ground state faster at lower temperatures, this is shown in figure 7.3

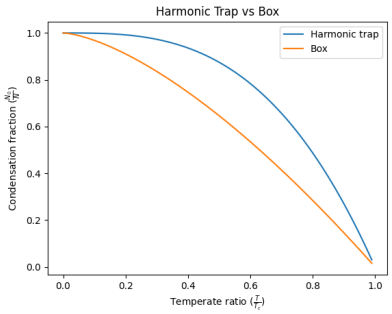

Figure 7.3: Comparison between condensation fraction in harmonic trap and box.

7.1.3 Gross-Pitaevskii Equation (GPE)

In section 1.3.1, a simple description non-interacting (ideal gas) boson gases trapped by a 3D harmonic oscillation potential was made. When dealing with gases that particles interact with each other (real gas), to do it, we employ the mean-field theory of Gross-Pitaevskii. This theory describes the properties of an interacting boson gas at absolute zero temperature, with the scattering length much smaller than the average distance between gas particles, ensuring that the loss of atoms from the Bose-Einstein condensate (BEC) to other quantum states of the system is negligible.

Considering a system of N bosonic particles described by the Hamiltonian:

$$H = \sum_{i=0}^{N}\left[\frac{p_i^2}{2m_i} + V\left(\vec{r_i}\right) + U_0\sum_{i<j}\delta\left(\vec{r_i} - \vec{r_j}\right)\right] \tag{7.21}$$

The first term represents it's kinetic energy, the second term the external potential, and the last term the interaction between particles, with U_0 representing the constant characterizing the effective contact potential between the particles. Here, we will consider repulsive interactions by adopting $U_0 > 0$.

In dilute atomic gases, interactions are primarily binary and can be theoretically treated as a scattering approximation of s-wave. The exact form of the interaction potential between particles is unknown, and only one parameter, denoted as "a," the scattering length of the s-wave, characterizes the interaction, where $U_0 = \frac{4\pi\hbar^2 a}{m}$ Let us construct the Hamiltonian operator:

$$\hat{H} = \sum_{i=0}^{N}\left[-\frac{\hbar^2}{2m_i}\nabla_i^2 + V\left(\vec{r_i}\right) + U_0\sum_{i<j}\delta\left(\vec{r_i} - \vec{r_j}\right)\right] \tag{7.22}$$

The energy functional for N particles system:

$$\left\langle\Phi\left(\vec{r_1}...\vec{r_n}\right)\right|\hat{H}\left|\Phi\left(\vec{r_1}...\vec{r_n}\right)\right\rangle = \int d\vec{r_1}... \\ ... \int d\vec{r_n}\Phi^*\left(\vec{r_1}...\vec{r_n}\right)\hat{H}\Phi\left(\vec{r_1}...\vec{r_n}\right) \tag{7.23}$$

Merging equation 7.22 and equation 7.23.

$$E = \int d\vec{r_1}... \int d\vec{r_n}\Phi^*\left(\vec{r_1}...\vec{r_n}\right) \\ \cdot\left\{\sum_{i=0}^{N}\left[-\frac{\hbar^2}{2m_i}\nabla_i^2 + V\left(\vec{r_i}\right) + U_0\sum_{i<j}\delta\left(\vec{r_i} - \vec{r_j}\right)\right]\right\}\Phi\left(\vec{r_1}...\vec{r_n}\right) \tag{7.24}$$

$$E = \sum_{i=0}^{N}\int d\vec{r_1}... \int d\vec{r_n}\Phi^* \\ \left(\vec{r_1}...\vec{r_n}\right)\left[-\frac{\hbar^2}{2m_i}\nabla_i^2 + V\left(\vec{r_i}\right) + U_0\sum_{i<j}\delta\left(\vec{r_i} - \vec{r_j}\right)\right]\Phi\left(\vec{r_1}...\vec{r_n}\right) \tag{7.25}$$

Using the Hartee approximation the above expression can be simplified into

$$\Phi\left(r_1\vec{...}\vec{r_n}\right) = \varphi(\vec{r_1})...\varphi(\vec{r_n})$$
$$\rightarrow E = \sum_{i=0}^{N}\int d\vec{r_1}...\int d\vec{r_n}\left[\varphi(\vec{r_1})...\varphi(\vec{r_n})\right]^*$$
$$\left[-\frac{\hbar^2}{2m_i}\nabla_i^2 + V\left(\vec{r_i}\right) + U_0\sum_{i<j}\delta\left(\vec{r_i}-\vec{r_j}\right)\right]\varphi(\vec{r_1})...\varphi(\vec{r_n}) \tag{7.26}$$

$$E = \sum_{i=0}^{N}\int d\vec{r_i}\varphi^*(\vec{r_i})$$
$$\left[-\frac{\hbar^2}{2m_i}\nabla_i^2 + V\left(\vec{r_i}\right) + U_0\sum_{i<j}\int\delta\left(\vec{r_i}-\vec{r_j}\right)\left|\varphi(\vec{r_j})\right|^2 d\vec{r_j}\right]$$
$$\varphi(\vec{r_i}) \tag{7.27}$$

$$E = \sum_{i=0}^{N}\int d\vec{r_i}$$
$$\left[-\frac{\hbar^2}{2m_i}\varphi^*(\vec{r_i})\nabla_i^2\varphi(\vec{r_i}) + V\left(\vec{r_i}\right)\varphi^*(\vec{r_i})\varphi(\vec{r_i}) + ...\right]$$
$$\left[... + \frac{N-1}{2}U_0\left|\varphi(\vec{r_i})\right|^2\varphi^*(\vec{r_i})\varphi(\vec{r_i})\right] \tag{7.28}$$

Since:

$$\int -\varphi^*(\vec{r_i})\nabla_i^2\varphi(\vec{r_i})d\vec{r_i} = -\left[\varphi^*(\vec{r_i})\nabla_i\varphi(\vec{r_i})\right]_{|\vec{r_i}|\rightarrow\infty}$$
$$+\int\nabla_i\varphi^*(\vec{r_i})\nabla_i\varphi(\vec{r_i})d\vec{r_i} = 0 + \int\nabla_i\varphi^*(\vec{r_i})\nabla_i\varphi(\vec{r_i})d\vec{r_i} \tag{7.29}$$

Then, equation 7.28 becomes:

$$E = \sum_{i=0}^{N}\int d\vec{r_i}$$
$$\left[\frac{\hbar^2}{2m_i}\nabla_i\varphi^*(\vec{r_i})\nabla_i\varphi(\vec{r_i}) + V\left(\vec{r_i}\right)\varphi^*(\vec{r_i})\varphi(\vec{r_i}) + ...\right]$$
$$\left[... + \frac{N-1}{2}U_0\left|\varphi(\vec{r_i})\right|^2\varphi^*(\vec{r_i})\varphi(\vec{r_i})\right] \tag{7.30}$$

$$E = N\int d\vec{r}\left[\frac{\hbar^2}{2m}\left|\nabla\varphi(\vec{r})\right|^2 + \frac{N-1}{2}U_0\left|\varphi(\vec{r})\right|^4\right]d\vec{r} \tag{7.31}$$

Then the solution becomes:

$$E = N\int d\vec{r}.$$
$$\cdot\left[\frac{\hbar^2}{2m}\left|\nabla\varphi(\vec{r})\right|^2 + V(\vec{r})\left|\varphi(\vec{r})\right|^2 + \frac{N-1}{2}U_0\left|\varphi(\vec{r})\right|^4\right]d\vec{r} \tag{7.32}$$

By defining the wave function of the condensate as a whole:

$$\psi(\vec{r}) = \sqrt{N}\varphi(\vec{r}) \rightarrow n(\vec{r}) = \left|\psi(\vec{r})\right|^2 \tag{7.33}$$

Since $n(\sim r)$ is the spatial numerical density, by using a large N where $N-1 \approx N$, the following conclusion can be made:

$$N = \int\left|\psi(\vec{r})\right|^2 d\vec{r} \rightarrow E =$$
$$\int\left[\frac{\hbar^2}{2m}\left|\nabla\psi(\vec{r})\right|^2 + V(\vec{r})\left|\psi(\vec{r})\right|^2 + \frac{1}{2}U_0\left|\psi(\vec{r})\right|^4\right]d\vec{r} \tag{7.34}$$

$$E = \int\left[-\frac{\hbar^2}{2m}\psi^*(\vec{r})\nabla^2\psi(\vec{r}) + V(\vec{r})\psi^*(\vec{r})\psi(\vec{r}) + ...\right]$$
$$\left[... + \frac{1}{2}U_0\left[\psi^*(\vec{r})\psi(\vec{r})\right]^2\right]d\vec{r} \tag{7.35}$$

Assuming $L = E - \mu N$.

$$L = \int\left[-\frac{\hbar^2}{2m}\psi^*(\vec{r})\nabla^2\psi(\vec{r}) + \left[V(\vec{r})-\mu\right]\psi^*(\vec{r})\psi(\vec{r}) + ...\right]$$
$$\left[... + \frac{1}{2}U_0\left[\psi^*(\vec{r})\psi(\vec{r})\right]^2\right]d\vec{r} \tag{7.36}$$

Using Lagrange method, the minimum energy in relation of ψ^* can be established

$$\frac{\partial L}{\partial\psi^*} = \frac{d}{dt}\left(\frac{\partial L}{\partial\dot{\psi^*}} = 0\right)$$
$$\rightarrow -\frac{\hbar^2}{2m}\psi^*(\vec{r})\nabla^2\psi(\vec{r}) + \left[V(\vec{r})-\mu\right]\psi^*(\vec{r})\psi(\vec{r}) + \frac{1}{2}U_0\left[\psi^*(\vec{r})\psi(\vec{r})\right]^2 \tag{7.37}$$

Thus arriving at the Gross-Pitaevskii independent-time equation:

$$-\frac{\hbar^2}{2m}\nabla^2\psi(\vec{r}) + V(\vec{r})\psi(\vec{r}) + U_0\left|\psi(\vec{r})\right|^2\psi(\vec{r}) = \mu\psi(\vec{r}) \tag{7.38}$$

This theory is an approximation and therefore not universally valid. Once the loss of atoms to other quantum states of the system becomes significant, this approximation is no longer valid. Throughout the derivation, we assume that the only interaction present among particles is the contact interaction, which means that this approximation holds true for dilute gases (where $na^3 \ll 1$) at absolute zero temperature ($T = 0K$).

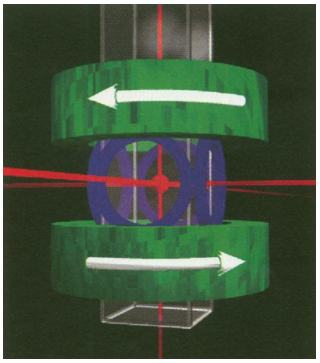

Figure 7.4: Schematic of the apparatus. Six laser beams intersect in a glass cell, creating a magneto-optical trap (MOT). The cell is 2.5 cm square by 12 cm long, and the beams are 1.5 cm in diameter. The coils generating the fixed quadrupole and rotating transverse components of the TOP trap magnetic fields are shown in green and blue, respectively. The glass cell hangs down from a steel chamber (not shown) containing a vacuum pump and rubidium source. Also not shown are coils for injecting the rf magnetic field for evaporation and the additional laser beams for imaging and optically pumping the trapped atom sample.

7.1.4 Visualization of BCE

Observation of a BECs

The article **Observation of Bose-Einstein condensation in a dilute atomic vapor**, a BEC was produced in a vapor of rubidium-87 atoms that was confined by magnetic fields and evaporatively cooled. This experiment was important because it provided direct evidence for the existence of Bose-Einstein condensation.

In the experiment, a cloud of rubidium-87 atoms was cooled using laser cooling techniques and a combination of lasers and magnetic fields. This cooling process brought the atoms to extremely low temperatures. Once sufficiently cooled, the atoms were transferred into a magnetic trap created by electromagnetic fields to prevent them from escaping. To achieve Bose-Einstein condensation, an evaporative cooling, selectively removing the highest-energy atoms from the trap, which gradually formed a condensate as the remaining atoms with lower energies coalesced. The presence of the condensate was confirmed through laser imaging techniques that allowed visualization of its density distribution by shining a laser beam through the atom cloud.

By setting $T = 170nK$ and $\frac{N}{V} = 2.5 \times 10^{12} cm^3$ three BCEs were observable.

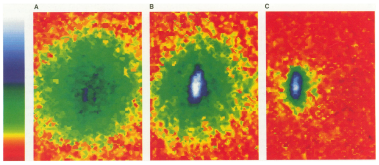

Figure 7.5: False-color images display the velocity distribution of the cloud (**A**) just before the appearance of the condensate. (**B**) just after the appearance of the condensate, and (**C**) after further evaporation has left a sample of nearly pure condensate. The circular pattern of the noncondensate fraction (mostly yellow and green) is an indication that the velocity distribution s isotropic, consistent with thermal equilibrium. The condensate fraction (mostly blue and white) is elliptical. indicative that it is a highly nonthermal distribution. The elliptical pattern is in fact an image of a single, macroscopically occupied quantum wave function. The field of view of each image is 200 Jm by 270 ipm. The observed horizontal width of the condensate is broadened by the experimental resolution.

3D visualization of BECs

The thesis by Smaira, titled "Quantum fluids spatial distribution evaluation and its characterization," explores the use of tomography to recon-

struct a Bose-Einstein condensate (BEC) in three dimensions. Tomography, a technique commonly employed in medical diagnostics and other scientific fields, allows for the creation of cross-sectional images of objects or body parts. By acquiring multiple projections of the object from different angles and utilizing computer algorithms, the internal structure of the object can be visualized.

In the case of Bose-Einstein condensates, the thesis showcases both a two-dimensional image (Figure 7.6) and a three-dimensional reconstruction (Figure 7.7).

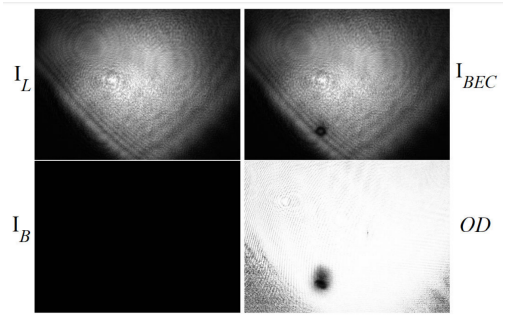

Figure 7.6: 2D images of BECs. Only laser beam (I_L), sample (I_{BEC}), background (I_B) and optical denstity (OD) images.

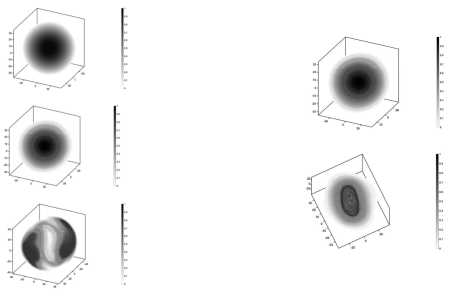

Figure 7.7: 3D reconstruction of BECs. On the left, from top to bottom, shows the Original 3D reconstruction, the reconstructed 3D cloud, and the difference between them. On the right, from top to bottom, shows the recovered 3D reconstruction and the Original cloud obtained from the experiment.

7.2 Conclusion

In conclusion, this article has provided a comprehensive overview of the distinctions between Fermions and Bosons, shedding light on the intriguing realm of Bose-Einstein condensates (BECs) and exploring some of their notable applications. The examination of an ideal Bose gas trapped by a three-dimensional harmonic potential highlighted the advantages of utilizing such a confinement method over a simple box. It became evident that the particles exhibited a significantly enhanced condensation rate within the harmonic potential.

Moreover, leveraging the insights gained from the three-dimensional harmonic example, this article also delved into the derivation of the Gross-Pitaevskii Equation, which underscores the disparity between dealing with ideal gases and real gases in the context of BECs. This distinction is crucial for a more comprehensive understanding of the behavior and properties of Bose-Einstein condensates in practical scenarios.

To complement the theoretical discussion, two visualizations were presented in this work. The first visualization, originating from a 1995 article, offered a groundbreaking glimpse into the emergence of BECs, marking a significant milestone in the field. The second visualization involved the reconstruction of BECs in three dimensions using computational methods, providing a contemporary perspective on the advances made in the visualization and study of these unique quantum phenomena.

Bibliografia

[1] Anderson, M. H., Ensher, J. R., Matthews, M. R., Wieman, C. E., & Cornell, E. A. (1995). Observation of Bose-Einstein condensation in a dilute atomic vapor. *Science*, 269(5221), 198-201.

[2] Smaira, A. F. (2015). Dinâmica de um condensado de Bose-Einstein contendo sólitons [Dissertação]. São Carlos: Universidade de São Paulo, Instituto de Física de São Carlos. Retrieved from `https://doi.org/10.11606/D.76.2015.tde-02042015-170017`. (Accessed: 2023-06-19)

[3] Bradley, C. C., Sackett, C. A., Tollett, J. J., & Hulet, R. G. (1995). Evidence of Bose-Einstein condensation in an atomic gas with attractive interactions. *Physical Review Letters*, 75(9), 1687.

[4] Smaira, A. F. (2019). Quantum fluids spatial distribution evaluation and its characterization [Tese]. São Carlos: Instituto de Física de São Carlos. Retrieved from `https://doi.org/10.11606/T.76.2019.tde-18052020-145912`. (Accessed: 2023-06-19)

8

Elitzur and Vaidman bomb testing problem

Vinícius Pereira Pinto

Instituto de Física de São Carlos, Universidade de São Paulo, 13560-970 São Carlos, SP, Brazil

Abstract: The Elitzur and Vaidman bomb testing problem is a thought experiment in quantum mechanics that explores the concept of quantum superposition and entanglement. In this experiment, a bomb is placed inside a chamber that has two entrances, each with a photon detector. The bomb is designed to either explode or not depending on the polarization of the photon that enters the chamber. However, the experiment is set up in such a way that it is impossible to know whether the bomb has exploded or not without disturbing the system. In this work, we propose a methodology that uses computer simulations to investigate the behavior of the system and also an experimental proposal that uses simple laser sources to test the theory.

8.1 Introduction

Quantum mechanics, as a foundational theory, provides a comprehensive framework for understanding the behavior of particles at the microscopic level. While numerous concepts contribute to the richness of this theory, two crucial aspects that challenge classical intuitions are superposition and entanglement. Delving into these ideas leads us to the fascinating concept of nonlocality in quantum mechanics.

Superposition refers to the remarkable phenomenon in which a particle can exist in multiple states simultaneously. Unlike classical objects, which are typically confined to definite properties, such as position or momentum, quantum particles can be in a state that encompasses a range of possibilities. This is exemplified by the famous Schrödinger's cat thought experiment [1], where the state of a cat is envisioned as a superposition of the dead and alive states until its state is observed.

Entanglement, on the other hand, reveals a profound correlation between particles that defies classical explanations. When two or more particles become entangled, their states become intertwined, regardless of the distance between them. Measurements made on one particle instantaneously affect the state of the other, irrespective of the spatial separation. This concept, famously described as "spooky action at a distance" by Einstein, Podolsky, and Rosen [2], challenges our classical intuition that information cannot travel faster than the speed of light.

To explore the implications of superposition and entanglement further, Elitzur and Vaidman devised the bomb test problem as a thought experiment [3]. The problem is set up as follows: A bomb is placed inside a chamber that has two entrances, each with a photon detector. The bomb is designed to either explode or not depending on the polarization of the photon that enters the chamber. However, the experiment is set up in such a way that it is impossible to know whether the bomb has exploded or not without disturbing the system. This is because the photon that enters the chamber is in a superposition of two polarizations, and the system becomes entangled with the bomb. This experiment raises the question of how to know whether the bomb has exploded or not without actually disturbing the system.

8.2 Bomb-testing problem

The Elitzur and Vaidman experiment consists of a Mach-Zehnder interferometer setup, consisting of beam splitters with reflectivity R, to explore the wave-particle duality of light and the concept of quantum superposition. In this experiment,

a single-photon light source is employed, ensuring that only one photon is emitted at a time. The experiment begins with the photon reaching the first beam-splitter, which divides the incoming light equally into two paths: path A (upper) and path B (lower). Each path is equipped with mirrors that redirect the photon towards the final beam-splitter.

The configuration of the interferometer is such that, under normal conditions, the beams interfere constructively at one of the detectors, referred to as D1, while they interfere destructively at the other detector, D2. This implies that when both paths are unobstructed, we expect to detect the photon exclusively at D1. This behavior aligns with classical expectations, as the constructive interference leads to a higher probability of detecting the photon at D1.

However, here's where the experiment becomes intriguing. Elitzur and Vaidman introduce a clever twist: they propose a specific set of conditions where one of the paths can be intentionally blocked. Remarkably, even when a path is obstructed, the experiment reveals a counterintuitive result. Instead of detecting the photon only at D1, as expected from classical reasoning, the experiment demonstrates that an equal amount of light is detected at both detectors, D1 and D2. To add drama, they propose that the path is blocked by a bomb that is triggered by a photodetector when it absorbs a single photon, as depicted in Figure (8.1).

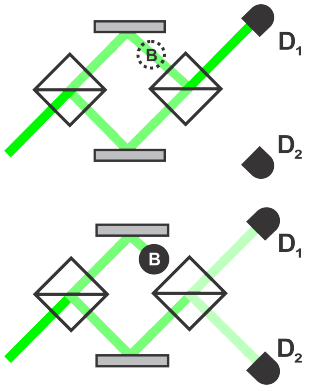

Figure 8.1: Elitzur-Vaidman experiment without the bomb (top) and with the bomb (bottom). Adapted from Koppell et al (2022).

In the case of single photon emissions, the outcomes of the interferometer can be categorized as follows:

- **No detector clicks:** This outcome occurs when the emitted photon interacts with an object placed in the path of the beam, preventing the photon from reaching any of the detectors. In this scenario, the presence of the object obstructs the photon's path, leading to the absence of any detection.
- **Detector D1 clicks:** This outcome can occur in two situations. Firstly, when the object is present in the path of the photon, causing it to interact and redirect to D1. Secondly, even in the absence of the object, D1 may still register a detection. Therefore, when D1 clicks, it indicates that the measurement has not succeeded and necessitates another attempt to obtain conclusive results.
- **Detector D2 clicks:** This is the desired outcome, as it signifies the measurement of the presence of an object without directly interacting with it, unlike in the first case. The occurrence of a detection at D2 suggests the absence of any obstruction in the path of the photon, indicating the likely presence of the object being measured.

Importantly, it is crucial to emphasize that the presence of an object can be reliably inferred only when a detection occurs at D2. This is due to the experimental setup, which is configured to yield destructive interference at D2. The destructive interference ensures that a detection at D2 can only be attributed to the presence of the object, as any obstruction in the photon's path would result in a different outcome.

Using the quantum mechanical formalism, we can describe the state of a photon moving down as $|1\rangle$ and up as $|2\rangle$. Let's assume a beam-splitter with reflectivity a for $|1\rangle$ and b for $|2\rangle$. Then, the operation for the beam-splitter is

$$\begin{aligned} |1\rangle &\xrightarrow{BS} \tfrac{1}{\sqrt{2}}(|1\rangle + i\,|2\rangle) \\ |2\rangle &\xrightarrow{BS} \tfrac{1}{\sqrt{2}}(|2\rangle + i\,|1\rangle) \end{aligned} \tag{8.1}$$

and the operation for a mirror is

$$\begin{aligned} |1\rangle &\xrightarrow{M} i\,|2\rangle \\ |2\rangle &\xrightarrow{M} i\,|1\rangle \end{aligned}. \tag{8.2}$$

When the object is absent in the system, as example A in Figure 8.1, the evolution is

$$\begin{aligned} |1\rangle &\xrightarrow{BS} \frac{1}{\sqrt{2}}(|1\rangle + i\,|2\rangle) \xrightarrow{M} \frac{1}{\sqrt{2}}(i\,|2\rangle - |1\rangle) \\ &\xrightarrow{BS} \frac{1}{2}(i\,|2\rangle - |1\rangle) - \frac{1}{2}(|1\rangle + i\,|2\rangle) \\ &= -\,|1\rangle \end{aligned}$$

In this case only detector D1 clicks, with probability 1.

If there is an object in the path, the photon can be absorbed, described by the state $|s\rangle$. Then the evolution will be given by

$$|1\rangle \xrightarrow{BS} \frac{1}{\sqrt{2}}(|1\rangle + i\,|2\rangle) \xrightarrow{M} \frac{1}{\sqrt{2}}(i\,|2\rangle + i\,|s\rangle)$$
$$\xrightarrow{BS} \frac{1}{2}(i\,|2\rangle - |1\rangle) + \frac{1}{\sqrt{2}}\,|s\rangle\,.$$

We then have that the detectors will collapse this quantum state into

$$|1\rangle \xrightarrow{Bomb\ test} \begin{cases} |1\rangle\,, & \text{D1 clicks, probability} = 1/4 \\ |2\rangle\,, & \text{D2 clicks, probability} = 1/4 \\ |s\rangle\,, & \text{no clicks, probability} = 1/2 \end{cases}$$

Thus, we can predict that the D2 detector only clicks when there is an object in the path, in this case the photon makes a measurement without interacting with the object in 25% of the measurements.

The success rate of interaction-free measurements can be quantified by the ratio of the probability of detecting the object and the sum of the probabilities of detection and of the photon being absorbed by the object:

$$\eta_{\,\mathrm{EV}} = \frac{P(\mathrm{det})}{P(\mathrm{abs}) + P(\mathrm{det})} \tag{8.3}$$

If 50/50 beam-splitters are used in the experiment, we have $P(\mathrm{det}) = 1/4$ and $P(\mathrm{abs}) = 1/2$, therefore $\eta_{\,\mathrm{EV}} = 1/3$. In the general case, for beam splitters with reflectivity R, we have $\eta_{\,\mathrm{EV}} = (1-R)/(2-R)$, which tends to the limit $\eta_{\,\mathrm{EV}} \leq 0.5$.

8.3 Interaction-Free Mesuramment

Since Elitzur and Vaidman's proposal, further advances have been made in the field of non-interaction measurements with the goal of increasing the 25% chance of detecting the bomb without actually interacting with it. One notable line of research involves using the Zeno effect to increase the probability of making measurements without direct interaction, reaching probabilities close to 100%.

The Zeno effect, named after the ancient Greek philosopher Zeno of Elea, refers to the phenomenon where frequent observations or measurements can significantly delay or even halt the evolution of a quantum system. This effect can be observed when

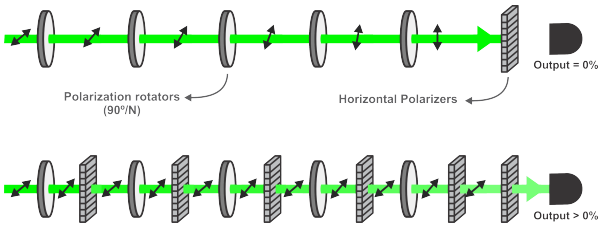

Figure 8.2: Horizontal polarization of a photon passing through N polarization rotators (90^{o}/N rotation each) converts it to vertical polarization, leading to its blockage by the horizontal polarizer (top). Inserting a horizontal polarizer after each rotator inhibits the polarization change, enabling light detection beyond the horizontal polarizer (bottom).
Adapted from Venugopalan (2007).

horizontally polarized light is passed through polarization rotators. In one scenario, a single measurement is made after the light passes through a horizontal polarizer at the end, resulting in a measurement intensity of 0%. In another scenario, measurements are taken at each rotation, yielding non-zero measurements, as depicted in Figure 8.2.

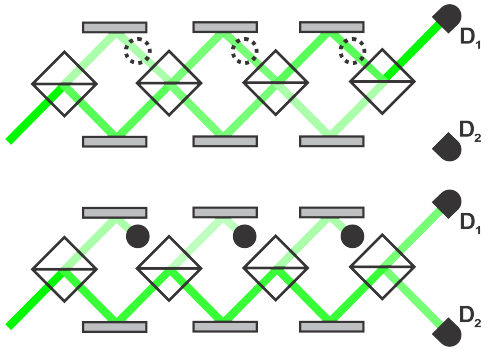

Figure 8.3: Variation of the Elitzur-Vaidman bomb testing problem with repeated tests known as interaction-free measurement.
Adapted from Koppell et al (2022).

In the context of the EV problem, the Zeno effect can be harnessed to increase the probability of successfully detecting an object without interacting with it. Several years later, Kwiat, Weinfurter, Herzog, Zeilinger, and Kasevich [5] proposed a different method that enables an increase in $\eta_{\,\mathrm{EV}}$ close to unity. Their approach involves passing a single photon through the Mach-Zender interferometer multiple times, where the photon gradually transitions from the lower left to the upper right half of the system, as illustrated in Figure 8.3. By introducing detectors at each cycle, the probability of detection increases via the "down" port of the final beam

splitter, indicating the presence of the object.

By incorporating detectors at each cycle, the photon acquires a probability, $P = \cos^2(\pi/2n)$, where n represents the number of cycles, to persist along the lower path. Evidently, the probability of the photon emerging through the lower exit after n cycles is given by:

$$P = \left[\cos^2\left(\frac{\pi}{2n}\right)\right]^n. \tag{8.4}$$

As the value of n increases ($n \geq 4$), the likelihood of achieving interaction-free measurements surpasses 50% of the maximum probability in the original EV setup [5]. Moreover, as n becomes larger, the proximity to an efficiency parameter, $\eta_{\text{EV}} = 1$, is attained.

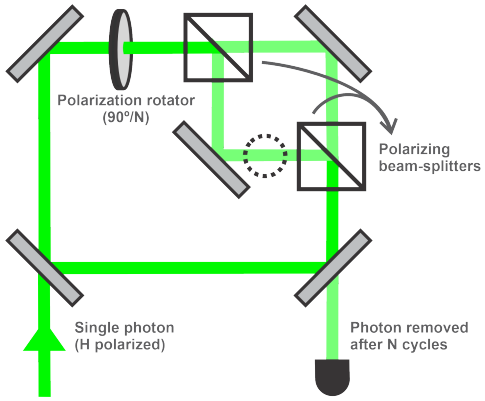

Figure 8.4: Variation of the Elitzur-Vaidman bomb test problem using a cavity for n repetitions of the injected single-photon.

Adapted from Kwiat.

Another approach involves injecting a single photon into a cavity to conduct the test multiple times, utilizing only one object instead of multiple objects as in the previous proposal. This method can be implemented by passing the photon through the same Mach-Zender interferometer for n iterations, as depicted in Figure 8.4, or by employing a Fabry-Perot resonator as an alternative [5, 6]. These experimental setups also serve to explore quantum eraser phenomena using interaction-free measurements [6].

8.4 Experiments

To qualitatively observe the experiment proposed by Elitzur and Vaidman, a Mach-Zender interferometer was constructed using two 50/50 beam-splitters and a HeNe laser operating at a wavelength of 632.8 nm, as illustrated in Figure 8.5.

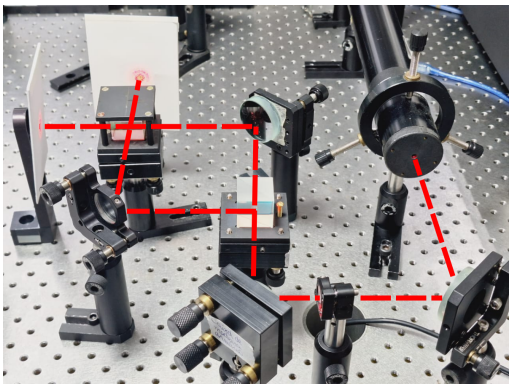

Figure 8.5: Reproduction of the original experimental setup of the Elitzur and Vaidman bomb testing problem using a Mach-Zender interferometer with two beam-splitters with reflectivity R = 50% (up); and interference patterns observed by the interferometer (bottom).

Elaborated by the author.

During the setup of the experiment, it becomes evident that when both paths are unobstructed, an interference pattern emerges at one output, while the complementary interference pattern arises at the other. However, when one of the paths is blocked by an object, the interference pattern vanishes, resulting in the previously darkened region becoming illuminated, as illustrated in Figure 8.6.

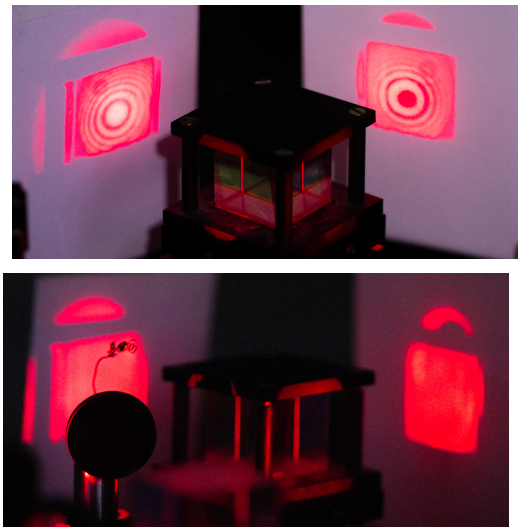

Figure 8.6: Comparison between the original EV experiment with no object in the path (up) and with an object in the path (bottom).

Elaborated by the author.

8.5 Simulations

The EV problem can also be investigated through experiments using quantum circuits implemented via high-level programming languages on commercially available gate-based superconducting quantum processors, such as those provided by IBM [7].

By employing a quantum circuit with two qubits, representing the photon and the bomb, we can utilize a Hadamard gate (H) to split the initial state $|q_0\rangle = |0\rangle$ into $|0\rangle$ and $|1\rangle$, encoding the which-path information. Subsequently, a CNOT gate entangles $|q_0\rangle$ with the target qubit $|q_1\rangle$, simulating the role of the bomb. Treating $|q_0\rangle$ as the signal, a second Hadamard gate is applied to probe the interference patterns. The desired outcome of this EV experiment relies on the state $|00\rangle$, indicating a successful interaction-free measurement. As depicted in Figure 8.7, we observe that $|00\rangle$ is obtained in 25% of the measurements.

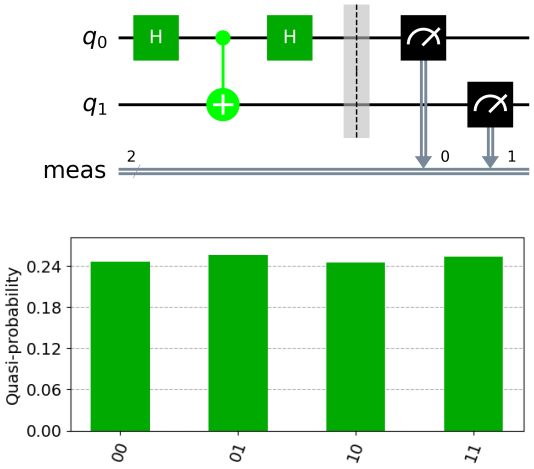

Figure 8.7: Quantum circuit for the original EV experiment, using the H gate to represent a 50/50 beam-splitter and a C-NOT gate to represent the bomb; and quantum circuit quasi-probabilities using IBM's cloud-based quantum computing service (Qiskit Runtime).

Elaborated by the author.

To enhance the success rate of interaction-free measurements, we can construct a quantum circuit employing n rotation operators, specifically R_x gates, which perform single-qubit rotations around the x-axis by an angle of θ/n (in radians) instead of using the Hadamard gate. In this configuration, as the number of cycles increases, the probability of achieving interaction-free measurements improves. Consequently, for sufficiently large values of n, we can approach an efficiency parameter of $\eta_{\text{EV}} = 1$, as illustrated in Figure 8.8.

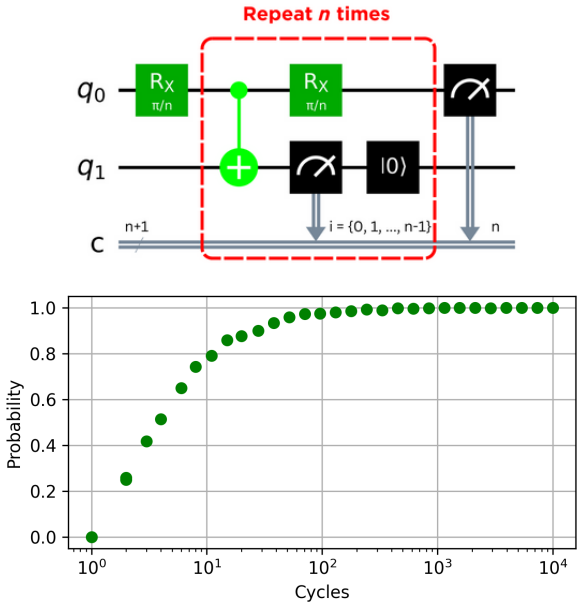

Figure 8.8: Quantum circuit for the interaction-free measurement experiment proposed by [5] for n cycles, where the $R_x(\pi/n)$ replaces the H gate for control over the reflectivity; and experimental data of quantum circuits from 1 to 10000 cycles using cloud-based quantum computing service by IBM (Qiskit Runtime).

Elaborated by the author.

8.6 Discussion

This puzzling outcome arises from the wave-particle duality inherent in quantum mechanics. Due to the superposition principle, the single photon simultaneously exists in both paths A and B until a measurement is made. Blocking one of the paths introduces an "either-or" scenario: if the blocked path is chosen, the photon must be in the unblocked path, and vice versa. Consequently, the photon appears to exhibit an intriguing property called "quantum nonlocality," where its presence in one path seems to affect the measurement outcome at the other detector.

By carefully controlling the experimental conditions and analyzing the detection probabilities at D1 and D2, Elitzur and Vaidman effectively demonstrate a quantum "interaction-free measurement." This peculiar phenomenon offers insights into the nature of quantum superposition and provides a

unique perspective on the counterintuitive behaviors exhibited by quantum systems.

8.7 Interpretations

The Elitzur-Vaidman bomb test experiment raises intriguing questions about the interpretations of quantum mechanics. Various perspectives have been proposed to explain the outcomes of the experiment, each offering unique insights into the fundamental nature of quantum phenomena.

One interpretation focuses on the notion of a "single real result." It suggests that the measurement outcome corresponds to the actual interaction between the photon and the bomb. The experiment demonstrates that a conclusive result can be obtained without direct interaction, challenging classical intuitions regarding measurement processes [3]. Another aspect explored in the context of the experiment is the violation of Bell inequalities. These mathematical inequalities provide a criterion to assess the presence of non-local correlations in entangled systems [9]. The violation observed in the experiment suggests the existence of non-local influences, highlighting the non-classical nature of quantum entanglement.

The interpretation known as Bohmian mechanics offers an alternative perspective. It proposes the existence of hidden variables that determine the particle's trajectory, even in the presence of superposition and entanglement. In the Elitzur-Vaidman experiment, this interpretation posits that the photon's path is guided by its interaction with the bomb, providing an explanation for the observed measurement outcomes [10].

On the other hand, the many-worlds interpretation introduces the concept of parallel universes. According to this interpretation, when the Elitzur-Vaidman experiment is conducted, the universe splits into different branches corresponding to each possible measurement result [11, 12]. Each branch represents a different reality where the photon interacts with the bomb or avoids it and the results of the experiment can be understood as the observer's experience in one of the many coexisting parallel worlds. Therefore, this interpretation says that when the observer manages to predict that there is a bomb without interacting with it, the photon was absorbed into another universe and the bomb did indeed explode.

These interpretations offer diverse and thought-provoking explanations for the outcomes of the Elitzur-Vaidman bomb test. They deepen our understanding of the intricate nature of quantum mechanics and its implications for the nature of reality, measurement, and the behavior of quantum systems. By exploring these interpretations, we gain valuable insights into the profound and enigmatic aspects of the quantum world.

8.8 Conclusion

The bomb test problem illustrates the nonlocal nature of entanglement in quantum mechanics. The ability to obtain information about a particle's state at a remote location, through the entanglement with another particle, implies a connection that transcends traditional notions of spatial distance and challenges our understanding of causality. While the exact mechanisms behind this nonlocality are still a subject of ongoing research and debate, experimental observations have consistently confirmed the validity of entanglement and its influence on distant particles.

These remarkable insights into the nonlocal nature of entanglement hold profound implications for the advancement of quantum technology. Exploiting entanglement has the potential to revolutionize fields such as quantum communication, quantum cryptography, and quantum computing. It was even a topic that earned the researcher Anton Zeilinger, quoted here, the Nobel Prize for applying these concepts in experiments with entangled photons, establishing the violation of Bell inequalities and pioneering quantum information science. For instance, entanglement-based protocols enable secure and efficient quantum key distribution, facilitating secure communication over long distances. Moreover, the ability to manipulate and control entangled particles is a fundamental requirement for quantum computation, where quantum bits (qubits) exhibit superior computational capabilities compared to classical bits. Consequently, understanding and harnessing the nonlocality of entanglement not only enriches our understanding of quantum mechanics but also drives innovations in quantum technology with transformative implications for various scientific and technological domains.

Bibliografia

[1] Schrödinger, Erwin. "Die gegenwärtige Situation in der Quantenmechanik". *Naturwissenschaften*, **23** (48): p. 807–812, (1935).

[2] A. Einstein, B. Podolsky, and N. Rosen, "Can quantum-mechanical description of physical reality be considered complete?". *Phys. Rev.*, **47**, p. 777, (1935)

[3] Elitzur, Avshalom C.; Lev Vaidman. "Quantum mechanical interaction-free measurements". *Foundations of Physics*, **23** (7): p. 987–997 (1993).

[4] Koppell, Stewart et al. "Transmission electron microscopy at the quantum limit". *Appl. Phys. Lett.*, **120** (19), (2022)

[5] Kwiat, P. G. ; Weinfurter, H.; Herzog, T.; Zeilinger, A.; Kasevich, M. A. "Interaction-free Measurement". *Phys. Rev. Lett.*, **74** (24): p. 4763–4766 (1995).

[6] Karlsson, A.; Björk, G.; Tsegaye, T. "Theory of interaction-free measurements in cavity resonators". *J. Opt. Soc. Am. B* **15** (12), 2958-2966 (1998)

[7] Tran, D. M.; Nguyen, D. V.; Le, B. H.; Nguye, H. Q. "Experimenting quantum phenomena on NISQ computers using high level quantum programming", *EPJ Quantum Technology* **9**: 6 (2022)

[8] Venugopalan, Anu. "The quantum Zeno effect—watched pots in the quantum world". *Resonance*, **12** (4): p. 52-68, (2007)

[9] Leifer, M. S., "Is the Quantum State Real? An Extended Review of ψ-ontology Theorems". *Quanta*, **3** (1): 67, (2014).

[10] Bricmont, J., "The de Broglie–Bohm Theory", *Making Sense of Quantum Mechanics*, p. 129–197, (2016).

[11] Vaidman, L., "On the Paradoxical Aspects of New Quantum Experiments". *Philosophy of Science Association 1994*, p. 211–217, (1994).

[12] McQueen, K. J.; Vaidman, L., "In Defence of the Self-Location Uncertainty Account of Probability in the Many-Worlds Interpretation". *Studies in History and Philosophy of Science*, **66**: p. 14–23, (2019).